ACS EARTH AND SPACE CHEMISTRY

http://pubs.acs.org/journal/aesccq

Article

Discerning Poly- and Monosaccharide Enrichment Mechanisms: Alginate and Glucuronate Adsorption to a Stearic Acid Sea Surface Microlayer

Maria G. Vazquez de Vasquez, Mickey M. Rogers, Kimberly A. Carter-Fenk, and Heather C. Allen*

Cite This: https://doi.org/10.1021/acsearthspacechem.2c00066

Read Online

ACCESS | Metrics & More | Article Recommendations | Supporting Information

ABSTRACT: Poly- and monosaccharides are ubiquitous in the marine environment and are enriched in sea spray aerosol but the mechanisms for their enrichment are not fully understood. We expand upon previously defined co-adsorption mechanisms by investigating the co-absorption of alginate and its representative monomeric form, glucuronate, to a stearic acid monolayer as a function of saccharide concentration on an ocean proxy solution. Using Langmuir isotherms, surface-sensitive infrared reflection−absorption spectroscopy, and Brewster angle microscopy, we demonstrate that the mechanism of co-adsorption significantly differs between alginate and glucuronate. We find that film thickness increases from ∼3.5 to 4.8 nm and from ∼3.5 to ∼3.7 nm upon co-adsorption of alginate and glucuronate to stearic-d_{35} acid monolayers, respectively, indicating that alginate forms multilayers underneath the monolayer. Glucuronate shows a different co-adsorption where it likely intercalates and induces significant reorganization within the monolayer. We quantify the Langmuir adsorption coefficients and half-saturation concentrations of both alginate and glucuronate co-adsorption to stearic-d_{35} acid. We find that alginate co-adsorption produces the Langmuir adsorption constants $K_{alginate}$ = 0.089 ± 0.015 and $C_{1/2,alginate}$ = 11 ± 1.9 mg/L alginate and glucuronate co-adsorption produces $K_{glucuronate}$ = 0.081 ± 0.015 and $C_{1/2,glucuronate}$ = 12 ± 2.3 mg/L glucuronate. Thus, we demonstrate that the use of monosaccharides alone as a proxy for saccharide enrichment is insufficient, and we provide important parameters for better representation of saccharides in marine aerosol investigations.

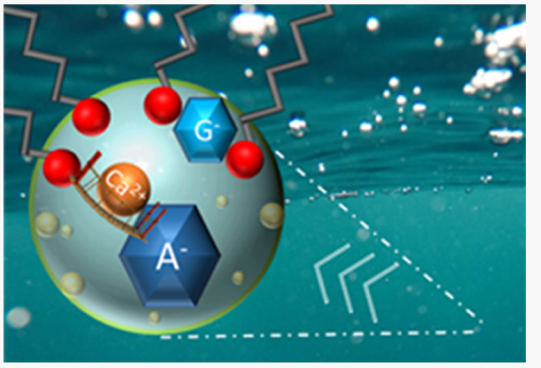

KEYWORDS: *half-saturation concentrations, adsorption coefficient, saccharides, Brewster angle microscopy, infrared spectroscopy*

INTRODUCTION

Poly- and monosaccharides can comprise a significant fraction of organic carbon in sea spray aerosol (SSA) depending upon the season and biological activity in the ocean.[1,2] Estimates have shown that up to 61% of SSA content by mass comes from saccharides with the greatest saccharide enrichment observed in submicron SSA.[3−5] Saccharide enrichment in SSA starts with breaking waves entraining air bubbles that become coated in surface-active organic matter derived from marine biota.[1,4,6−9] The adsorbed biogenic organic matter is sprayed into the atmosphere upon bubble bursting.[8,10,11] Yet, the exact transport mechanism of saccharides from bulk seawater to the sea surface microlayer (SSML) remains understudied,[12] causing an underestimation of saccharide presence in SSA.[6,7,13] Atmospheric processes in the marine boundary layer are dependent upon SSA composition.[14−21] SSA containing saccharides, particularly those within marine microgels, comprise an important fraction of cloud condensation nuclei (CCN)[22−25] and ice nucleating particles (INPs),[26−33] thus affecting cloud formation and albedo. Clouds and ice are important regulators of the overall radiative budget on Earth, scattering and absorbing solar radiation. Changes in SSA composition alter the abundance of cloud condensation nuclei and ice nucleating particles, which ultimately drive climate processes, like temperature and weather, in the marine boundary layer.[3,34−38] Without accurate measures of saccharide content within SSA, studies will be based on underestimated values, limiting our accurate understanding of saccharide enrichment.

In the SSML, polysaccharides can aggregate into gels that can influence the interfacial reactivity.[39−43] These marine gels are three-dimensional polymer networks hydrated by seawater. Typically, gels cannot disperse if they are covalently linked, but gels that are interlinked via ionic and hydrophobic interactions are much more responsive to changes in the chemical environment.[44] Usually, marine gels are cross-linked by Ca^{2+}

Received: March 4, 2022
Revised: May 6, 2022
Accepted: May 9, 2022

ions with a random tangled topology, and such organization can be changed by temperature and pH. Previous Brewster angle microscopy (BAM) studies revealed that filtered dissolved organic matter less than or equal to 200 nm in size self-assembles.[39,45] Free polymeric dissolved organic matter likely reaches a critical concentration at the air−water interface, leading to polymer rafts that collapse into nanogels. These nanogels then diffuse into the bulk subphase and further aggregate to form microgels.

Previous studies have discussed the electrostatic interactions between saccharides and lipid headgroups, calculated the enrichment of saccharides, and measured surface propensity.[46] However, the exact mechanics of such interactions and enrichment had yet to be defined.[12] Recent findings from Hasenecz et al. showed a specific enrichment of the polysaccharide alginate in proxy SSA samples that was further enhanced (EF = 1.6 to 2.4) upon the addition of $CaCl_2$ to the subphase.[47] Alginate is a highly abundant oceanic compound produced by *Phaeophyta* or brown algae.[48] Specifically, alginate is the most abundant polysaccharide produced by brown algae and accounts for 15−60% of its dry weight.[49] Alginate is a linear anionic polysaccharide that provides structural function within the cell walls of brown algae.[50] Some bacteria, such as *Pseudomonas*, can synthesize alginate, as well.[51] However, most marine bacteria depolymerize algal-based alginate via alginate and oligoalginate lyase enzymes and eventually to its monomeric form.[49,52] Herein, alginate serves as a vital substrate for bacterial metabolism and a source of oligosaccharides and monosaccharides, which can also enrich the SSML and SSA environments. Poly-, oligo-, and monosaccharides are all readily available to interact with oceanic salts, such as $CaCl_2$, which has been shown to facilitate bridging to such saccharides, co-adsorbing them to the air−water interface.[53]

Recent work from Carter-Fenk et al. measured a cationic bridging mechanism in which alginate co-adsorbs to a deprotonated fatty acid monolayer, providing new insights into the enrichment process of saccharides at the air−water interface.[54] Ca^{2+} facilitates the greatest extent of alginate co-adsorption among other oceanic-relevant cations such as Na^+ and Mg^{2+}. This work is foundational in providing empirical parameters to improve the representation of polysaccharides in the sea surface microlayer. While polysaccharide representation and mechanistic transfer to the aerosol environment are becoming better established in the literature, monosaccharides may not maintain the same complexity and mechanics as polysaccharides and require their own systematic studies to quantify their surface propensity. Saccharide content in the SSML and SSA was measured throughout two phytoplankton blooms by Jayarathne et al. and found that enrichment factors of monomers hydrolyzed from oligo-/polysaccharides were ∼1−16 and ∼14−1314 for SSML and submicron SSA, respectively.[3] Studies are therefore needed to understand the mechanistic transfer of monomers to the SSA environment to help explain such enrichment.

In this study, we expand upon the cationic bridging mechanism that drives alginate co-adsorption to deprotonated monolayers by studying glucuronic acid, a commercially available analogue to mannuronic acid and guluronic acid, as it is representative of the monomeric form of alginate. We measured the Langmuir adsorption coefficient and half-saturation concentration of both alginate and glucuronate to stearic-d_{35} acid monolayers using surface-sensitive infrared reflection−absorption spectroscopy (IRRAS). Langmuir surface pressure−area (Π−A) isotherms, in combination with infrared reflection−absorption spectroscopy, provide structural insights within the stearic-d_{35} acid monolayers. Brewster angle microscopy (BAM) and non-equilibrium relaxation (NER) studies provide the means to calculate monolayer thickness as a function of saccharide concentration. We observe adsorption of alginate to an insoluble monolayer via cationic bridging, whereas our monomeric studies using glucuronate suggest co-adsorption via intercalation. Our data of alginate and glucuronate co-adsorption to a deprotonated monolayer suggests that monomer glucuronate surface propensity is a contributor to saccharide composition but cannot model alginate polysaccharide representation in SSA.

EXPERIMENTAL METHODS

Materials. Stearic acid (octadecanoic acid, $CH_3(CH_2)_{16}COOH$, >99%, Sigma-Aldrich) and deuterated octadecanoic acid (stearic-d_{35} acid, $CD_3(CD_2)_{16}CO_2H$, >98%, Sigma-Aldrich) were used as received. Stearic acid is a surface-active molecule and is found to be the second most abundant fatty acid (with palmitic acid being the first) in marine samples.[55] Stearic acid is an insoluble surfactant in water, having a water(in)-solubility of ∼0.00029/100 g at 20 °C.[56] The air−water interface gives rise to preferred orientations of these surface-active molecules such that the hydrophobic portion persists in the air phase and the hydrophilic portion interacts with the solution phase making stearic acid a good proxy for monolayer formation. The compounds were dissolved in chloroform (HPLC grade, Fisher Scientific) to prepare ∼1.5 mM solutions. Calcium chloride dihydrate (Certified ACS, Fisher Chemical) was used as received. Sodium chloride (Certified ACS, Fisher Chemical) was baked for at least 10 h in a furnace at 650 °C to remove residual impurities.[57,58] Alginic acid (sodium salt, ACROS Organics, Lot: A0406891) and glucuronic acid (sodium salt monohydrate. 99% ACROS Organics, Lot: A0397856) were used as received from the same batch to maximize homogeneity in molecular composition. All aqueous solutions were prepared with nanopure water with a resistivity of 18.2 MΩ·cm (Milli-Q Advantage A10, EMD Millipore) in glassware cleaned with a piranha acid bath.[54,58,59] The aqueous solutions consisted of constant marine water concentrations of 476 mN NaCl and 10 mM $CaCl_2$ and a varying concentration of alginate or glucuronate ranging from 0 to 100 mg/L to a total volume of 1 L. The ionic composition was selected to model the concentration of the most abundant and enriched cations in seawater, without complicating spectral interpretation, while maintaining high ionic strength as in seawater. The nanopure water has a pH of 5.6 ± 0.1 due to atmospheric CO_2 acidification.[58,60] Atmospheric CO_2 also acidifies the proxy aqueous solution, so the solutions were initially pH adjusted to 8.7 ± 0.1 to ensure that the pH will be approximately 8.2 ± 0.1 throughout the experimental measurements. The solution pH was adjusted by adding microliter aliquots (∼72−100 μL) of 0.345 M NaOH solution made from sodium hydroxide pellets (98% extra pure, ACROS Organics) in nanopure water. The aqueous subphase solution pH was measured before and after experiments. During this study, no unexpected or unusually high safety hazards were encountered.

Langmuir Surface Pressure−Area Isotherms. All Langmuir surface pressure−area (Π−A) isotherms were performed in the same Teflon Langmuir trough with an area

https://doi.org/10.1021/acsearthspacechem.2c00066
ACS Earth Space Chem. XXXX, XXX, XXX−XXX

of 148.8 cm^2 fitted with movable Delrin barriers (KSV NIMA, Finland). The volume of the trough is 135 mL with a depth of ~1 cm. Π−A isotherms provide insights into the overall monolayer structure, intermolecular interactions, and the co-adsorption of alginate and glucuronate. Surface pressure was measured using a platinum Wilhelmy plate. The Wilhelmy plate, trough, and barriers were thoroughly cleaned with reagent alcohol (Histological grade, Fisher Scientific) and nanopure water and dried before each trial. The Wilhelmy plate was flamed using a hot flame of a Bunsen burner by holding the plate in the hottest part of the flame for a few seconds until the plate glows red hot to remove residual organics. After the aqueous solution consisting of a constant concentration of 476 mN NaCl and 10 mM $CaCl_2$ and a ranging concentration from 0 to 100 mg/L (step size of 10 mg/L) of alginate or glucuronate was added to the trough, its surface was checked for contamination by compressing the barriers and ensuring that the surface pressure did not rise above 1.0 mN/m. The stearic acid solution prepared in chloroform was spread dropwise onto the aqueous surface to form a monolayer using a microsyringe (Hamilton, 50 μL). The chloroform solvent was allowed to evaporate for 10 min. The barriers were symmetrically compressed at a rate of 5 mm/min/barrier. As the barriers are compressed (reducing the area with the barriers) at a constant rate, changes in surface pressure are measured as a function of the surface area available to each molecule (mean molecular area, MMA). A number of distinct regions are immediately apparent in examining the isotherm. The regions are called phases, which are identified as discontinuities in the isotherm. The phase behavior of a monolayer is mainly determined by the physical and chemical properties of an amphiphile, the subphase (aqueous solution) temperature, and the subphase composition. During the isotherm compression, Brewster angle microscopy images were taken every 4.85 s (see the Brewster angle microscopy method section for more details). The microsyringe was cleaned thoroughly between each trial with reagent alcohol, set to dry, and then rinsed 8−10 times with chloroform.

Brewster Angle Microscopy. The same Langmuir trough was used during the Brewster angle microscopy (BAM) imaging. These experiments were performed using a custom-built setup,[18,60−62] which further allowed for visualization of the air−aqueous interface during compression Langmuir surface pressure−area (Π−A) isotherms. BAM imaging provides morphological evidence of monolayer structural changes. The BAM setup is mounted on a goniometer, which allows for adjusting the angle of incidence to the Brewster angle of the aqueous solution, ~53°, from the surface normal for pure water. The 1.5 mW He-Ne laser source (Research Electro-Optics, Boulder, CO) emits polarized light at a wavelength of 543 nm with linear polarization. The p-polarized light goes through a Glan-laser calcite polarizer for further purification before being reflected off the aqueous surface.[18,62] The reflected light is then collected and collimated by a 10× infinity-corrected superlong working distance objective lens (CF160 Tu Plan EPI, Nikon Instruments, Melville, NY) and a tube lens (MXA22018, Nikon, instruments, Melville, NY; focal length 200 mm) to collect the collimated beam before going into a back-illuminated EM-CCD camera (iXon DV887-BV, Andor Technology, Concord, MA; 512 × 512 active pixels with 16 μm x 16 μm pixel size). Before the stearic acid was spread onto the solution of interest (constant concentrations of 467 mM NaCl and 10 mM $CaCl_2$ and changing concentrations of 0−100 mg/L alginate or glucuronate), an image of the background solution was taken to ensure a gray level of 30 or less. Once this was calibrated, stearic acid was spread onto the solution of interest and the experiment was started and an image was recorded every 4.85 s. The BAM images were processed using ImageJ software (version 1.52a, National Institute of Health, Bethesda, MD) and cropped from their original size to show the region of the highest resolution. The dark regions of the BAM images correspond to the aqueous surface or to the less condensed phases of the surfactant, whereas the bright regions correspond to surfactant-rich areas. In this work, BAM was also utilized during the Π−A isotherm and the non-equilibrium relaxation (NER) experiments.

Infrared Reflection−Absorption Spectroscopy. Infrared reflection−absorption spectroscopy (IRRAS) measurements were performed using a custom-built optical setup[63−67] to measure the co-adsorption of alginate and glucuronate to a stearic-d_{35} acid monolayer as a function of saccharide concentration. Two planar gold mirrors at 48° relative to the surface normal were placed inside a Fourier transform infrared spectrometer (FTIR) (Frontier, PerkinElmer). The incident unpolarized beam is reflected off the input gold mirror and onto the surface, where the beam interacts with the interface and then reflects the output mirror and finally to the liquid nitrogen-cooled HgCdTe (MCT) detector. Spectra were collected with polarized light as an average of 400 scans in the single-beam mode with a resolution of 4 cm^{-1} within the range of 4000−450 cm^{-1} in 0.5 cm^{-1} increments. IRRAS spectra of stearic-d_{35} acid were collected and spread to the condensed phase in a Petri dish with a subphase solution volume of 20 mL at a mean molecular area of 20 $Å^2$/molecule onto the aqueous solutions of constant 467 mM NaCl and 10 mM $CaCl_2$ concentrations with a varying concentration of alginate or glucuronate (0−100 mg/L, low regime 0, 0.5, 5, and 10 mg/L and higher regime from 10 to 100 mg/L with a step size of 10 mg/L). Reflectance−absorbance (RA) spectral baseline was corrected using a linear or a fourth-order polynomial in the region of interest. Peak integration was also used. Both processes were performed using OriginPro 9. The OH stretching region was analyzed by fitting a line between 3000 and 3800 cm^{-1} for baseline subtraction, and the area under the curve was integrated between these points. Reported Langmuir adsorption coefficients and half-saturation concentration errors incorporate both spectral and fitting uncertainties.

The IRRAS spectra were analyzed in the OH stretching region (3000−3800 cm^{-1}), the COOH stretching region (1230−1800 cm^{-1}), and the CD_2 scissoring mode region (1070−1150 cm^{-1}). IRRAS spectra are plotted as reflectance−absorbance (RA) using eq 1,

$$\mathrm{RA} = -\log\left(\frac{R_{\mathrm{monolayer}}}{R_{\mathrm{proxy}}}\right) \tag{1}$$

where $R_{\mathrm{monolayer}}$ is defined as the reflectance of the monolayer and R_{proxy} is the reflectance of the bare aqueous solution surface.[68−72] Thus, only the spectral signal from the interfacial monolayer is captured. In our IRRAS spectra, both positive and negative peaks are observed. If the RA values are negative, then the reflectance of the monolayer is greater than the reflectance of the proxy aqueous solution ($R_f/R_0 > 1$). If the

https://doi.org/10.1021/acsearthspacechem.2c00066
ACS Earth Space Chem. XXXX, XXX, XXX−XXX

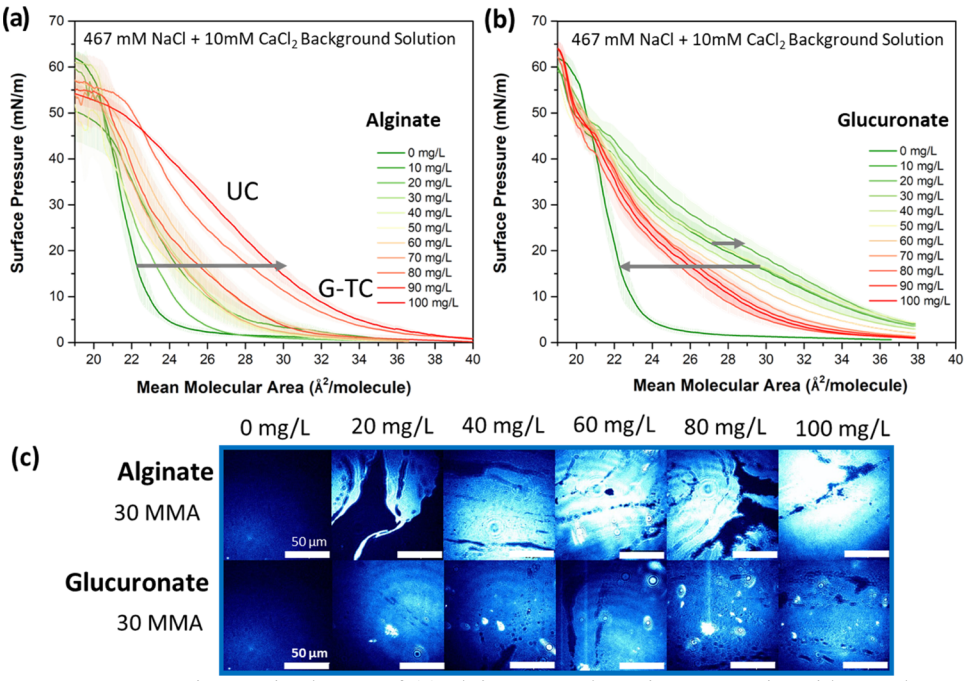

Figure 1. Langmuir Π−A isotherms of (a) alginate co-adsorption to the stearic acid monolayer at pH 8.2 at various alginate concentrations. (b) Glucuronate intercalation into the stearic acid monolayer at pH 8.2. (c) BAM images provide evidence of the alginate co-adsorption via Ca^{2+} bridging interactions and of the intercalation of glucuronate to the stearic acid monolayer. Additional BAM images of the full compression isotherms are shown in Figure S1. The scale bar in all images is 50 μm.

RA values are positive, then the reflected signal of the proxy aqueous solution is greater than that of the monolayer ($R_f/R_0 > 1$). Alginate and glucuronate were also included in the aqueous solution spectra (R_{proxy}) to isolate the alginate and glucuronate co-adsorbed to the stearic-d_{35} acid monolayer.

Monolayer Non-equilibrium Relaxation at a Constant Surface Pressure. The non-equilibrium relaxation (NER) experiments were also performed using the same Teflon Langmuir trough with an area of 148.8 cm^2 and a volume of 135 mL. Surface pressure was measured using a platinum Wilhelmy plate. The aqueous solutions contain constant 467 mM NaCl and 10 mM $CaCl_2$ with 0, 10, 20, 50, and 100 mg/L concentration of alginate or 0, 10, 20, 40, 50, and 100 mg/L concentration of glucuronate. The solution surface was checked for contamination as described in the Langmuir surface pressure−area isotherm methods. Stearic acid was then spread dropwise onto the solution of interest. The monolayers were compressed by symmetric compression of the trough barriers to a target surface pressure of 30 mN/m to ensure a full monolayer formation. The surface pressure was maintained by continuous motion of the barriers at a maximum rate of forward/backward motion of 1 mm/min/barrier. The change in the relative area (A/A_0) was then analyzed as a function of time.

RESULTS AND DISCUSSION

Probing Packing and Morphological Features of Co-adsorbed Poly- and Monosaccharides. Packing and morphological measurements were collected by Π−A isotherms in tandem with Brewster angle microscopy (BAM). Figure 1 informs on stearic acid monolayer organization while varying the concentration of either alginate or glucuronate in the subphase. Stearic acid was chosen due to its ocean relevance and prevalence in nascent sea spray aerosol.[14,55,73,74] Stearic acid is partially deprotonated at ocean pH (8.2), which is the pH at which these experiments were performed. Thus, the headgroup interaction and its hydration structure drive the differences in the Π−A isotherm measurements.[65]

All measurements were collected at room temperature (23.0 ± 1.0 °C). Each monolayer was analyzed over an aqueous solution of a constant NaCl and $CaCl_2$ background of 467 and 10 mM, respectively, with 11 varying alginate or glucuronate concentrations of 0−100 mg/L with a step size of 10 mg/L, as shown in Figure 1a,b. According to the literature, dissolved organic carbon concentrations are approximately 0.7−1 mg carbon/L.[47,75] The concentration of saccharides in the ocean is ∼20% of the dissolved organic carbon,[47,76] suggesting that saccharide concentration is ∼0.14−0.2 mg/L. The alginate and glucuronate concentrations used for the Π−A isotherms are ∼2−3 orders of magnitude greater than the saccharide concentration in dissolved organic, which maintains detectability within Π−A isotherms. Additionally, high concentrations are still relevant due to the evaporative process in aged sea spray aerosol.[1,47] Our Π−A isotherms are consistent with previous high-ionic-strength studies.[66,77−80] As the barriers compress the stearic acid monolayer to smaller mean molecular areas (MMAs), distinct regions are observed. These regions are referred to as phases, which are discontinuities in the surface pressure−area isotherms.[81,82] The film undergoes a smooth 2D phase transition, from gas-tilted condensed (G-TC) to an untilted condensed (UC) phase. The films reach maximum surface pressure between ∼50 and 60 mN/m for alginate and ∼60−65 mN/m for glucuronate. Such high surface pressure indicates that the stearic acid film on the aqueous solution is resistant to collapse. This phase behavior could be due in part to Coulombic repulsions between negative-charged carboxylic moieties and by contact ion pair formation between the carboxylate and

https://doi.org/10.1021/acsearthspacechem.2c00066
ACS Earth Space Chem. XXXX, XXX, XXX−XXX

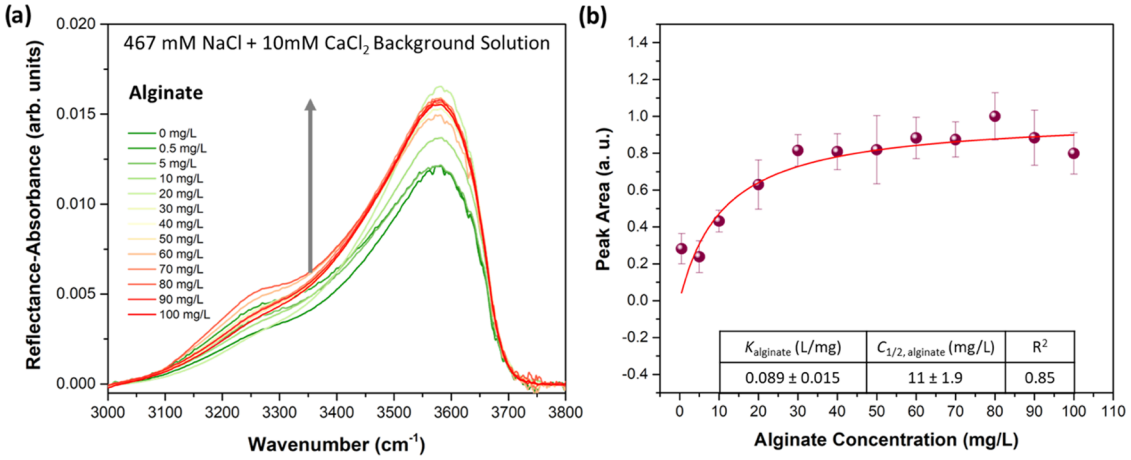

Figure 2. (a) IRRAS spectra of the ν(OH) indicating the significant alginate co-adsorption to the stearic-d_{35} acid monolayer at different concentrations. (b) Normalized peak area of the ν(OH) of alginate co-adsorption to the stearic-d_{35} acid monolayer. All scans have a constant aqueous solution concentration of 467 mM NaCl and 10 mM $CaCl_2$ with a changing alginate concentration (0−100 mg/L). The Langmuir co-adsorption coefficient, $K_{alginate}$, is given as (L/mg) and the half-saturation concentration, $C_{1/2,alginate}$, as mg/L. Error bars correspond to one standard deviation that has been propagated through the operations used in the normalization calculation.

Ca^{2+} cation.[83] The surface pressure plateau could alternatively be the result of the slow relaxation kinetics caused by the cohesive forces between the lipids.[80,84] When alginate is added to the proxy aqueous solutions (Figure 1a), the stearic acid monolayer expands monotonically as a function of alginate concentration. Thus, the Π−A isotherms suggest that alginate co-adsorbs to the interface, consistent with previous studies revealing that the mechanism for alginate enrichment or co-adsorption is via Ca^{2+} bridging to an insoluble monolayer.[47,54]

In the case of glucuronate (Figure 1b), we also observed monolayer expansion relative to the stearic acid monolayer spread in the absence of glucuronate. However, this expansion is not monotonic. The stearic acid monolayers on the 10−20 mg/L glucuronate solutions are the most expanded compared to the other concentrations. Upon the addition of just 10 mg/L of the monomer, there is a 6-fold increase in expansion of stearic acid for glucuronate compared to alginate. While alginate is a polysaccharide and made of several units of monosaccharides, we do not observe a large expansion proportional to its size increase. However, the drastic expansion, or increase in the surface area available to one molecule, increases disproportionately for the monomer glucuronate, strongly suggesting its presence at the interface and disrupting the packing[46] of stearic acid. This likely indicates intercalation of glucuronate to the interface, therefore altering the monolayer structure. Spectral evidence will be required to clarify if intercalation is occurring. At 50 mg/L glucuronate, directionality in the trend changes and lower MMAs are observed compared to the 10−20 mg/L glucuronate, suggesting monolayer rearrangement. Therefore, monolayer rearrangement is undergoing several potential processes: intercalation of glucuronate, stearic acid monolayer desorption, and cationic bridging. It is evident that the glucuronate mechanism of co-adsorption is very different than that of alginate. This also shows that glucuronate is not a valid proxy system for polysaccharide interactions as it does not exhibit a similar co-adsorption mechanism to an insoluble monolayer.

BAM images were taken simultaneously with the isotherms, showing the changes between alginate and glucuronate interaction with the monolayer. Increasing saccharide adsorption and monolayer thickness change the interfacial refractive index, thereby increasing the intensity of reflected light from the surface. From the alginate BAM images (Figure 1c (top)), we observe distinctive striations in addition to bright overall reflection, which supports the previously suggested divalent cation co-adsorption mechanism. However, stearic acid with glucuronate (Figure 1c (bottom)) shows dimer images overall with intensely bright spots, which are the likely formation of aggregates. The small bright spots, likely due to the formation of aggregates, suggest that the stearic acid monolayer undergoes a significant reorganization in the presence of glucuronate, as supported by the pivotal point from expansion to compression in the UC phase, as shown in Figure 1b. Additionally, one may expect that increasing the concentration of glucuronate will result in a multilayered interface with an increase in film thickness; however, this does not occur. Instead, the insignificant changes in brightness with increasing glucuronate concentration point to glucuronate intercalation into the monolayer, producing the observed reorganization. Based on these studies, we can argue that the co-adsorption mechanisms between alginate and glucuronate are inherently different.

Interfacial Infrared Reflection−Absorption of Alginate and Glucuronate. Studies have shown that polysaccharide enrichment is facilitated by divalent cationic bridging, and Ca^{2+} induces the greatest extent of alginate co-adsorption.[1,13,47,54,85] In this study, alginate and glucuronate co-adsorption to a stearic-d_{35} acid monolayer at constant ionic composition was experimentally investigated as a function of alginate or glucuronate concentration. The ionic composition of the subphase was selected to model concentrations of the most abundant and relevant cations and to account for high ionic strength as in seawater. This proxy consisted of 467 mM NaCl and 10 mM $CaCl_2$.[54,86,87] The alginate and glucuronate concentrations used in this spectroscopy experiment are ∼0.5−3 orders of magnitude higher than the saccharide concentration in dissolved organic, and such concentrations are close enough to remain relevant in the understanding of saccharide enrichment in the marine surface microlayer while facilitating confident interpretation of the physical mechanism driving alginate and glucuronate co-adsorption. Deuterated stearic acid

https://doi.org/10.1021/acsearthspacechem.2c00066
ACS Earth Space Chem. XXXX, XXX, XXX−XXX

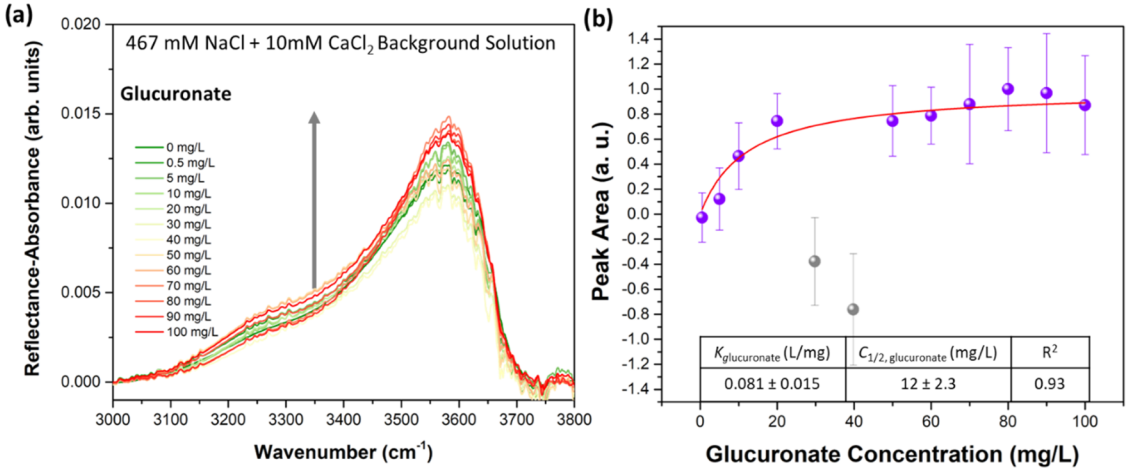

Figure 3. (a) IRRAS spectra of the ν(OH) region indicating glucuronate co-adsorption to a stearic-d_{35} acid monolayer at different concentrations. (b) Normalized peak area of the ν(OH) region of glucuronate co-adsorption to the stearic-d_{35} acid monolayer. All scans have a constant aqueous solution concentration of 467 mM NaCl and 10 mM $CaCl_2$ with a changing glucuronate concentration (0−100 mg/L). The gray spheres show the 30 and 40 mg/L glucuronate data points falling below the reflectance−absorbance value of the aqueous solution containing only the salts. The Langmuir co-adsorption coefficient, $K_{glucuronate}$, is given as (L/mg) and the half-saturation concentration, $C_{1/2,glucuronate}$, as mg/L. Error bars correspond to one standard deviation that has been propagated through the operations used in the normalization calculation.

was used to spectrally isolate the CD_2 scissoring mode from the carboxylate stretching region.[54,65,67,88] The protonation state of the carboxylic headgroup of stearic-d_{35} acid was maintained by adjusting the pH value of the subphase solutions from 5.6 to 8.2. The literature has shown surface pK_a shifts to higher values.[83,89−93] A reported surface pK_a of stearic acid is ∼10.15.[90] The pK_a values of the alginate monomers guluronic (G) and mannuronic (M) acids are 3.7 and 3.4, respectively.[94] Hence, at seawater pH of 8.2, stearic acid is partially deprotonated and alginate and glucuronate are completely deprotonated. Carboxylic acid deprotonation via salts has been shown at pH values significantly lower than the pK_a.[65−67,79,88,95−99]

Ca^{2+} Alginate Co-Adsorption Coefficient and Half-Saturation Concentration. In this study, the OH stretching region (ν(OH)) was used to quantify changes in interfacial coverage as a function of alginate co-adsorption. Figure 2a illustrates the changes in the ν(OH) due to the increase in surface coverage via alginate co-adsorption. The spectra show how increasing the alginate concentration increases the reflectance−absorbance value, ultimately increasing its co-adsorption to the stearic-d_{35} acid monolayer. The greatest ν(OH) signal enhancement happens around ∼3580 cm^{-1}. This region has been well-defined as the surface water molecules form hydrogen bonds with the carboxylic acid headgroup of a fatty acid.[65,89,97,100,101] As a result, alginate co-adsorption with increasing concentration enhances the signal around 3580 cm^{-1} because of the alginate carboxylate hydration.[65]

To quantify the co-adsorption of alginate to a stearic-d_{35} acid monolayer, the ν(OH) peak area of the film as a function of alginate concentration was fitted to a Langmuir adsorption isotherm. The Langmuir adsorption model is a well-known and accepted method for quantifying how an absorbate forms a layer on a given surface based on equilibration between the two phases.[102,103] The ν(OH) peak areas were quantified via peak area integration and normalized to values between zero and one. A value of 0 corresponds to the peak area of a 0 mg/L alginate solution where the solution only contains the aqueous proxy (467 and 10 mM $CaCl_2$) and a value of 1 corresponds to the highest peak area, coming from the 80 mg/L alginate in proxy aqueous solution where alginate co-adsorption to the monolayer is fully saturated. The reported errors correspond to one standard deviation and were propagated through the operations used in the normalization calculation. Because all ν(OH) peak areas are normalized to the peak area of a system containing only the background proxy aqueous solution without alginate, any normalized peak area greater than zero is attributed solely to alginate co-adsorption to the stearic-d_{35} acid carboxylate headgroup.

Considering the complete chemical system of insoluble surfactant and soluble saccharide, we employed Langmuir fitting to calculate adsorption constants. The spectroscopic results are plotted in Figure 2b as alginate concentration versus normalized peak area of ν(OH). The monolayer composition shows a positive correlation between the peak area and alginate concentration. The data is fit to a Langmuir model (eq 2) based on the work by Burrows et al. OCEANFILMS-2.[6,13,104]

$$A = A_{max}\frac{K_{sacc}C_{sacc}}{1 + K_{sacc}C_{sacc}} = A_{max}\frac{C_{sacc}}{C_{1/2,sacc} + C_{sacc}} \quad (2)$$

A and A_{max} are peak intensity and maximum peak intensity of ν(OH), C_{sacc} is the concentration of saccharide, K_{sacc} is the affinity coefficient for adsorption, and $C_{1/2,sacc}$ is the half-saturation concentration.[6,104] Therefore, we analyze and report the Langmuir adsorption coefficient and half-saturation concentration of alginate to the stearic-d_{35} acid monolayer. We find $K_{alginate}$ = 0.089 ± 0.015 L/mg and $C_{1/2,alginate}$ = 11 ± 1.9 mg/L, as shown in Figure 2b. Alginate exhibits a strong adsorption isotherm and reaches saturation at relatively low concentrations.

Glucuronate Co-Adsorption Coefficient and Half-Saturation Concentration. A similar analysis was performed for glucuronate, where the ν(OH) region, shown in Figure 3a, indicates that glucuronate is also being adsorbed to the stearic-d_{35} acid monolayer but to a lesser extent and possibly by a different co-adsorption mechanism. Based on the ν(OH) mode at ∼3580 cm^{-1}, it is evident that monolayer rearrangement is happening at concentrations of 30 and 40 mg/L glucuronates where the reflectance−absorbance values are less than the

https://doi.org/10.1021/acsearthspacechem.2c00066
ACS Earth Space Chem. XXXX, XXX, XXX−XXX

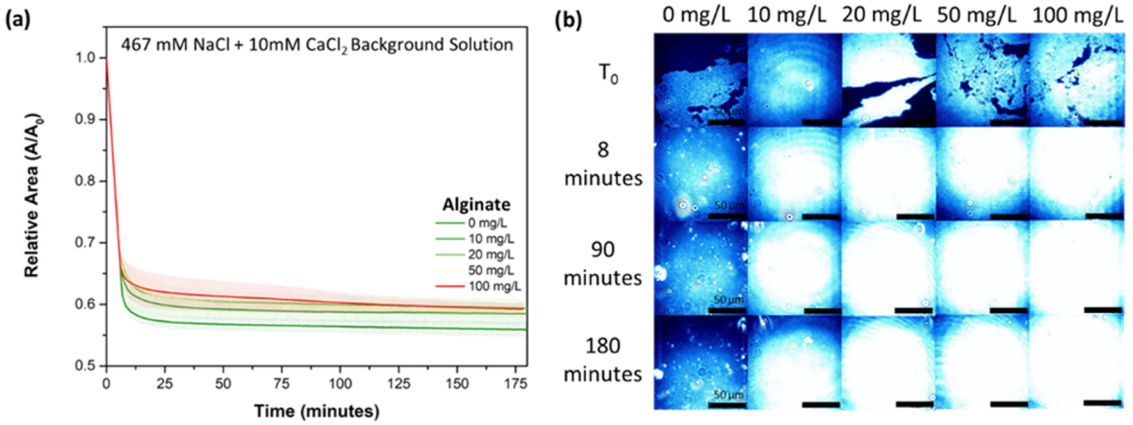

Figure 4. (a) Monolayer non-equilibrium relaxation at a constant surface pressure of a stearic acid monolayer onto a subphase aqueous solution containing a constant aqueous solution concentration of 467 mM NaCl and 10 mM $CaCl_2$ and a varying alginate concentration of 0, 10, 20, 50 and 100 mg/L. (b) BAM images of each monolayer at various times within the experiment.

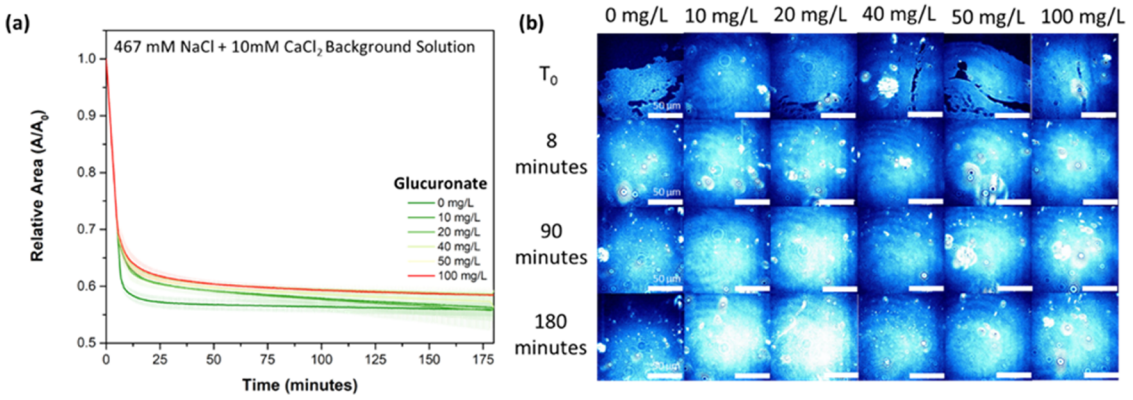

Figure 5. (a) Monolayer non-equilibrium relaxation at a constant surface pressure of a stearic acid monolayer onto a subphase aqueous solution containing a constant aqueous solution concentration of 467 mM NaCl and 10 mM $CaCl_2$ and a varying glucuronate concentration of 0, 10, 20, 40, 50, and 100 mg/L. (b) BAM images of each monolayer at various times within the experiment.

reflectance−absorbance value of just the monolayer spread on the proxy aqueous solution. Such a decrease in the reflectance−absorbance values could indicate different co-adsorption mechanisms caused by lipid desorption and/or monolayer rearrangement.

The ν(OH) region peak areas were also quantified via peak area integration and normalization between zero and one, as plotted in Figure 3b. Based on the normalized data in Figure 3b, the 30 and 40 mg/L glucuronate solutions are negative values relative to the 0 mg/L solution, suggesting that monolayer rearrangement and/or desorption occur at these particular glucuronate concentrations. While more sensitive instrumentation may be needed, we can speculate that the 30−40 mg/L concentration regime is the most immediate concentration following saturation. Thus, the Langmuir and BAM measurements indicate that glucuronate is unreliable as a proxy system for alginate and does not capture the complexity of the monolayer enrichment via co-adsorption of alginate. The Langmuir adsorption coefficient and the half-saturation concentration of glucuronate to the stearic-d_{35} acid monolayer were determined using the same model described above (Figure 3b). As the 30 and 40 mg/L glucuronate measurements are negative compared to the other concentrations, the fitting to the Langmuir adsorption model was inaccurate. To statistically remove these two concentrations from the fitting data, a residual analysis was performed; details are shown in the Supporting Information (SI) section in Figure S2 and Table S1. By the removal of these two concentrations from the normalized peak data, the fitting shows an R^2 value of 0.93. We also calculate $K_{glucuronate}$ = 0.081 ± 0.015 L/mg and $C_{1/2,glucuronate}$ = 12 ± 2.3 mg/L (Figure 2b). As expected, we observed a smaller Langmuir adsorption coefficient and half-saturation concentration for glucuronate. These quantitative adsorption parameters agree with our qualitative observations of weakened glucuronate co-adsorption to stearic acid monolayers via the Π−A isotherms and BAM images. Additionally, the IRRAS spectra corroborate the Π−A isotherm and BAM image evidence of glucuronate-induced film reorganization and possible desorption into the subphase. Based on our calculated $K_{alginate}$ = 0.089 L/mg and $K_{glucuronate}$ = 0.081 L/mg, we calculated the ΔG_{ads} using the molecular masses of alginate = 296,000 g/mol[105] and glucuronate = 234.14 g/mol. We obtained an alginate ΔG_{ads} = −41.8 kJ/mol ($Pb^{2+}\Delta G_{ads}$ = −43 kJ/mol)[105] and a glucuronate ΔG_{ads} = −24.07 kJ/mol. The obtained negative values indicate the spontaneous character of alginate co-adsorption to a stearic acid monolayer via strong calcium bridging. Whereas the less negative glucuronate value suggests that less spontaneous adsorption and possibly weaker interactions with the stearic acid are occurring. Therefore, these values suggest differences in adsorption mechanisms, being calcium bridging vs intercalation.

https://doi.org/10.1021/acsearthspacechem.2c00066
ACS Earth Space Chem. XXXX, XXX, XXX−XXX

Monolayer Thickness of Co-Adsorbed Alginate and Glucuronate at the Air–Water Interface. To temporally assess the co-adsorption of alginate and glucuronate to a stearic-d_{35} acid monolayer, non-equilibrium relaxation (NER) experiments at a constant surface pressure, 30 mN/m, coupled with BAM were used to calculate thickness as a function of alginate or glucuronate concentration. The NER experiments were performed for 3 h (details in the Methods section). While the NER experiment was running, BAM images were taken every 120 s for a total of 90 images per trial. Each NER experiment was performed in triplicate for 10, 20, 50, and 100 mg/L for each saccharide (Figures 4a and 5a). In addition, the NER of stearic acid on 40 mg/L glucuronate was measured to understand the anomalous peak area decrease in the IRRAS spectra. Our results from the underlying solution with alginate show that the stearic acid monolayer reflectivity enhances as the concentration of alginate is increased (Figure 4b), suggesting multilayered alginate adsorption under the monolayer. The T_0 images (Figures 4b and 5b) correlate to the first image taken as the monolayer is compressed to the desired surface pressure. We can see that as the concentration of alginate increases, higher reflectance is observed, which can be attributed to multilayers under the monolayer.

While we see the formation of a full stearic acid monolayer on varied glucuronate subphases, the changes in reflectivity are not as stark. We also observed a slight diminishing in the brightness at concentrations between 20 and 50 mg/L glucuronates (Figure 5b). Carter-Fenk et al. reports molecular dynamic simulations showing the lack of alginate intercalation into the monolayer. The MD simulations reveal the formation of a second layer beneath the fatty acid monolayer and suggest that Ca^{2+} likely serves as a bridge between the two COO^- moieties.[54] Glucuronate opposes this finding where it intercalates into the monolayer and does not form a second co-adsorbed layer.

To further characterize the changes in film morphology, we calculated the relative film thickness using the BAM image data. Using the refractive index of stearic acid (n_m = 1.430),[106,107] the relative thickness (d) can be determined from the following equation[108] used to model ultrathin films (<20 nm)[109]

$$d = \frac{\lambda\sqrt{R_p}}{\pi \sin(2\theta_B - 90)} \frac{n_m^2(n_a^2 - n_s^2)}{\sqrt{n_a^2 + n_s^2}(n_a^2 - n_m^2)(n_s^2 - n_m^2)} \quad (3)$$

In this equation, λ is the laser wavelength, R_p is the p-polarized reflectance obtained from BAM images (i.e., at 10 mg/L alginate, the p-polarization reflectance of the stearic acid monolayer is 3.88×10^{-6}), n_m is the refractive index of the stearic acid monolayer, and θ_B is the Brewster angle. The refractive indices of air and salt proxy are n_a = 1.00 and n_s = 1.334, respectively, where our proxy is defined by a proportionate average refractive index of the salt in our solution.[63,110]

The monolayer thickness, as a function of alginate and glucuronate concentration, in Figure 6 shows evidence of the co-adsorption of saccharides to the interface. It is clear that the co-adsorption of alginate causes a larger change in the monolayer thickness evidenced by the increase from ~3.5 nm ([alginate] = 0 mg/L) to ~4.8 nm ([alginate] = 100 mg/L). Previous studies have shown that the late stages of an algal bloom had an average thickness of ~5 nm.[111] Other studies of

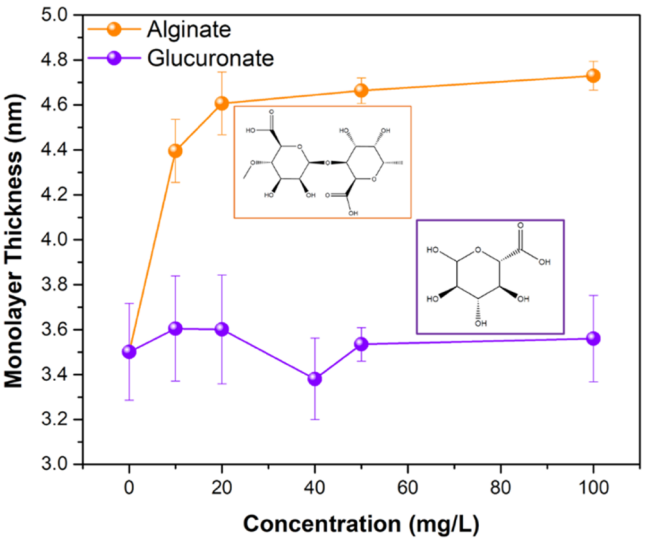

Figure 6. Film thickness of the co-adsorption of alginate (orange) and glucuronate (purple) to a stearic acid monolayer as a function of concentration. (The protonated form of the molecular structures is shown for reference).

relevant saturated long-chain fatty acids and phospholipids report an average thickness of ~1.3–3 nm, subject to the chemical composition of the subphase.[64] Surfactants spread on certain salts can dehydrate the carbonyl group and lengthen the thickness of the monolayer, as we observe an ~3.5 nm film thickness for stearic acid on the solution without alginate (Figure 6).[64] Our calculated thickness from alginate goes beyond the monolayer regime, indicating the presence of a multilayer film.[64,112,113] Aqueous solutions containing glucuronate show smaller changes, ranging from ~3.5 to ~3.7 nm, providing further evidence for minimal co-adsorption of glucuronate into a second layer at the interface. By using experimentally collected reflectivity, or albedo values, to calculate thickness, where our only assumption is the consistent maintenance of the interfacial refractive index, we have calculated values based on minimally assumed parameters that provide highly informative inputs for climate models. These results reveal the important influence of saccharide co-adsorption on the interface, thus suggesting that the role of monosaccharides as a proxy for a more complex system cannot provide a full picture of saccharide co-adsorption.

Impacts of Alginate versus Glucuronate Co-Adsorption on Stearic Acid Interfacial Structure. Fatty acid protonation states have an impact on the co-adsorption of alginate and glucuronate at the interface. A previous study demonstrated that there is less alginate co-adsorption at pH 5.8 than at basic pH (8.2).[54] It has been suggested that glucuronate ions bind to Ca^{2+} through three chelation sites.[114−116] Thus, for alginate and glucuronate co-adsorption to take place, the headgroup of the fatty acid has to be partially deprotonated. In addition to higher solution pH, previous work has shown that Ca^{2+} facilitates fatty acid headgroup deprotonation,[67,88,95,98,117,118] thereby increasing the number of potential Ca^{2+} bridging sites for alginate or glucuronate co-adsorption. Because the carboxylic spectral region (1230−1800 cm^{-1}) displays sensitivity to binding,[62,67,88,119,120] it is used to obtain additional insights into the co-adsorption of alginate,[54] glucuronate,[6,46,121] and the protonation state of the carboxylic headgroup of stearic-d_{35} acid.[67,88,95,96,117] Stearic-d_{35} acid

https://doi.org/10.1021/acsearthspacechem.2c00066
ACS Earth Space Chem. XXXX, XXX, XXX−XXX

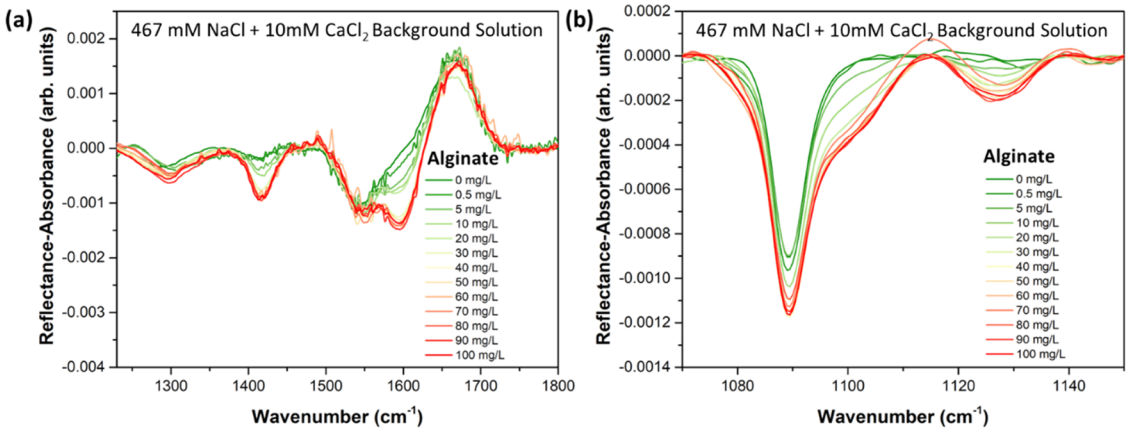

Figure 7. IRRAS spectra of the (a) COOH stretching region provide evidence of the alginate co-adsorption via Ca^{2+} bridging interactions to the stearic-d_{35} acid monolayer at pH 8.2. (b) δCD_2 mode region demonstrates the alginate co-adsorption to the stearic-d_{35} acid monolayer at pH 8.2. The spectra show no stearic-d_{35} acid lattice packing changes upon adsorption.

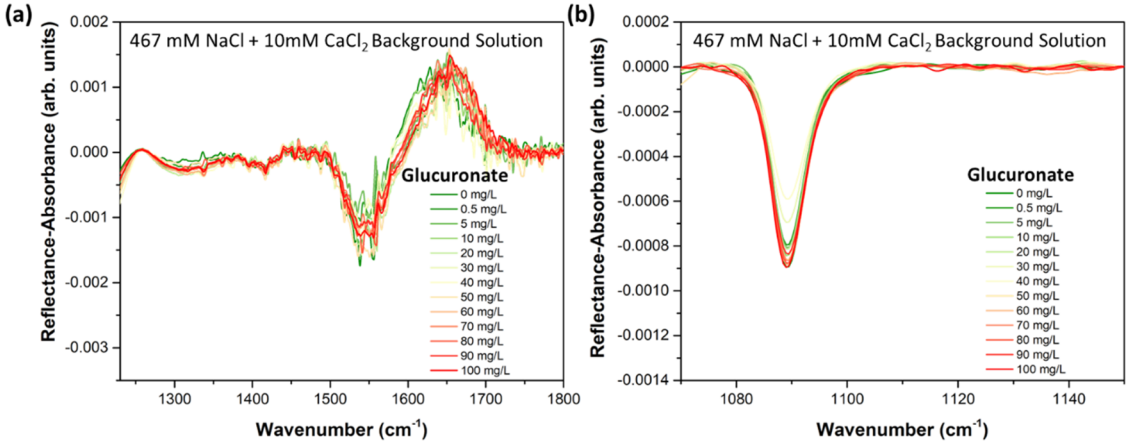

Figure 8. IRRAS spectra of the (a) COOH stretching region of the intercalation interaction of glucuronate to the stearic-d_{35} acid monolayer at pH 8.2. (b) δCD_2 mode region of the intercalation interaction of glucuronate to the stearic-d_{35} acid monolayer at pH 8.2. At 30 and 40 mg/L, a reduction in peak intensity is observed, possibly due to desorption of the stearic-d_{35} acid at these concentrations caused by monolayer rearrangement.

spread onto the proxy aqueous solution without alginate or glucuronate at pH 8.2 is deprotonated, as shown in Figures 7a and 8a by the presence of the asymmetric (ν_{AS}) (1500−1630 cm^{-1}) and symmetric (ν_S) (~1410 cm^{-1}) carboxylate (COO^-) modes and the disappearance of the carboxyl mode (~1720 cm^{-1}). As the alginate or glucuronate concentrations increase, the peak intensities of the $\nu_{AS}(COO^-)$ and $\nu_S(COO^-)$ modes increase. According to previous studies, this increase in intensity is due to co-absorption of alginate via divalent cationic bridging and the co-adsorption of glucuronate.[46,54]

Figure 7a shows each of the $\nu_{AS}(COO^-)$ and $\nu_S(COO^-)$ modes splitting into higher- and lower-frequency bands, where the higher-frequency COO^- bands have been previously assigned to the alginate carboxylate modes via harmonic vibrational frequency calculations.[54] Analogous peak enhancement and broadening were observed for the phosphate headgroup vibrational modes of 1,2-dipalmitoyl-*sn*-glycero-3-phosphatidic acid (DPPA) upon arginine and guanidinium binding.[62] Thus, the spectral signatures of fatty acid deprotonation are highly informative about the energetically favorable complexation between the lipid carboxylate headgroup, Ca^{2+}, and alginate. The spectra characterizing only the proxy seawater solution do not exhibit the high-frequency $\nu_{AS}(COO^-)$ mode. Upon the addition of alginate, a high-frequency band appears and increases as the concentration of alginate increases, providing direct spectroscopic evidence for alginate co-adsorption to the stearic-d_{35} acid monolayer. A more drastic increase in the alginate $\nu_{AS}(COO^-)$ mode intensity is observed between 10 and 30 mg/L, which is within the calculated half-saturation concentration from the Langmuir adsorption model. A blue shift is also observed for the stearic-d_{35} acid $\nu_{AS}(COO^-)$ mode. While this vibrational shift is not direct evidence of the alginate co-adsorption to the monolayer, it is possible that alginate disturbs the stearic-d_{35} acid headgroup hydration through electrostatic interactions with the headgroup.[79,122]

Interfacial film organization was also probed via the stearic-d_{35} acid δCD_2 mode (Figure 7b). All spectra exhibit a δCD_2 mode with a center wavelength of 1089 cm^{-1}, revealing that the hydrocarbon chains are packed in a hexagonal lattice structure.[123,124] The δCD_2 mode intensity also increases when the concentration of alginate is increased within the proxy aqueous solution. Such signal enhancement is most apparent at alginate concentrations above 10 mg/L, and it is particularly evident in the high-frequency regime. Through harmonic

https://doi.org/10.1021/acsearthspacechem.2c00066
ACS Earth Space Chem. XXXX, XXX, XXX−XXX

vibrational frequency calculations, Carter-Fenk et al. showed that the signal enhancement can be assigned to alginate ν, δ(C−O−H), ν(C−O−C), and C−H wagging modes.[54] Therefore, the signal enhancement adjacent to the δCD_2 mode is assigned to alginate co-adsorption via Ca^{2+} bridging with the carboxylate headgroup of stearic-d_{35} acid.

Hydrocarbon chain conformation of surfactants in a monolayer can also be determined by evaluating the ν_S, $\nu_{AS}(CD_2)$ center frequencies.[124] The CD_2 stretching region confirmed that the mechanism of alginate interfacial enrichment is by alginate Ca^{2+} bridging and not by intercalation of alginate into the stearic-d_{35} acid monolayer (Figure S3a). If alginate is intercalated into the stearic-d_{35} acid monolayer, changes in the CD stretching modes would be observed. Such intercalation would disrupt the monolayer, thus reducing the dispersion interactions between the alkyl tails, causing the CD stretching modes to blue shift. No spectral shifts were observed, ruling out intercalation and confirming that alginate is restrained to the surface region. Furthermore, the size of the alginate polysaccharide would prohibit intercalation between fatty acids within the monolayer.

When glucuronate is added to the proxy aqueous solution instead of alginate, the carboxyl region modes (1230−1800 cm^{-1}) do not increase in intensity (Figure 8a). The split of the asymmetric stretch (~1540 cm^{-1}) is not observed, suggesting that glucuronate Ca^{2+} bridging to the stearic-d_{35} acid headgroup is not the primary mechanism of enrichment. The lack of significant spectral changes with increasing glucuronate concentration shows that the interaction between the stearic-d_{35} acid monolayer and glucuronate is particularly different than its interaction with alginate. Studies have postulated that glucuronate enrichment at the interface occurs via co-adsorption.[6,46,85,121] While this is a possibility, our results suggest that glucuronate co-adsorption is not facilitated by divalent cationic bridging interactions. Thus, using glucuronate as a proxy system for saccharide co-adsorption will not fully capture alginate's mechanistic enrichment.

Because changes were not observed in the carboxyl region, we looked at the δCD_2 mode (Figure 8b). The δCD_2 mode centered at 1089 cm^{-1} reveals a hexagonal lattice structure. The enhancement observed for alginate is not present for glucuronate, again indicating the differing adsorption mechanisms for these two saccharides. Interestingly, we observed a decrease in the intensity of the δCD_2 mode at concentrations of 30 and 40 mg/L glucuronate, which is consistent with the shift from expansion to compression observed in the Π−A isotherms (Figure 1b), further supporting monolayer rearrangement and potential lipid desorption. The δCD_2 peak areas corresponding to 30 and 40 mg/L glucuronate diminish by ~20 and 30%, respectively (see Table S2 for peak area information). We also inspected the CD_2 stretching region (Figure S3b). While we did not observe any changes in the center wavelengths of the $\nu_S(CD_2)$ and $\nu_{AS}(CD_2)$ modes, we did observe a decrease in intensity of these two modes at 30 and 40 mg/L glucuronate. The $\nu_S(CD_2)$ and $\nu_{AS}(CD_2)$ modes decrease by 20% for the solution containing 30 mg/L glucuronate and 30% for the solution containing 40 mg/L glucuronate, which is consistent with the results of the δCD_2 mode. This reaffirms that monolayer rearrangement is occurring at these specific concentrations, suggesting that the monosaccharide enrichment mechanism requires future study. While our initial findings suggest that there are co-adsorption differences between polysaccharides and monosaccharides, we cannot comment extensively if these mechanistic differences will be transferable to other systems, thus future studies should be conducted using other polysaccharide and monosaccharide entities. However, we can state that the main driving force between alginate and glucuronate is size, impacting the co-adsorption mechanism, organization, and morphology within sea surface microlayer proxy films.

CONCLUSIONS

In this work, alginate and glucuronate co-adsorption interactions at a proxy sea surface microlayer were measured, compared, and quantified using Langmuir adsorption model fitting and film thickness analyses. We expand upon previous work characterizing the divalent cationic bridging mechanism driving alginate co-adsorption to deprotonated monolayers by studying glucuronic acid co-adsorption, as it is representative of the monomeric form of alginate. We measured the Langmuir adsorption coefficient and half-saturation concentration of both alginate and glucuronate to stearic-d_{35} acid monolayers using surface-sensitive infrared reflection−absorption spectroscopy (IRRAS). Langmuir surface pressure−area (Π−A) isotherms and IRRAS spectra provided insights into both the stearic-d_{35} acid monolayer and co-adsorbed saccharide structural organization at the air−water interface. Additionally, Brewster angle microscopy (BAM) and non-equilibrium relaxation (NER) studies provided further information on film morphology and monolayer thickness as a function of saccharide concentration.

We directly observe alginate co-adsorption to an insoluble monolayer via Ca^{2+} bridging and find that 11 ± 1.9 mg/L is the alginate half-saturation concentration. This represents the concentration at which half of the maximum of alginate co-absorption is reached. Alginate co-adsorption also increases film thickness, wherein the monolayer thickness increases from ~3.5 nm in the absence of alginate to a maximum thickness of ~4.8 nm at alginate co-adsorption saturation. Our results show that alginate reaches a strong adsorption to the interface at a relatively low concentration in the presence of Ca^{2+}. While we cannot directly compare our studies, we observe similar co-adsorption mechanisms. Hasenecz et al. observe alginate co-adsorption via cationic bridging demonstrated by the enhanced enrichment factor of alginate in aerosol from 1.6 to 2.4 upon the addition of calcium.[47] In our study, we also observed that the co-adsorption of alginate is dependent on its relative concentration. Monosaccharide enrichment was not studied in Hasenecz et al. as a function of calcium, however.

The monosaccharide glucuronate exhibits a strikingly different interplay between co-adsorption and intercalation into the stearic-d_{35} acid monolayer, resulting in an anomalous desorption and film reorganization for the 30 and 40 mg/L concentration studies, although this behavior does not persist for other glucuronate concentrations. We find 12 ± 2.3 mg/L to be the minimum concentration for glucuronate co-adsorption, indicating weaker glucuronate co-adsorption than that of alginate. Hasenecz et al. shows no monosaccharide enrichment at the interface.[47] The maximum film thickness of 3.7 nm suggests that glucuronate does not form a second layer underneath the lipid monolayer. Rather, the film morphological changes shown in the BAM images point to a glucuronate intercalation mechanism in the monolayer, yielding significant monolayer reorganization.

Our detailed study of alginate and glucuronate co-adsorption to a deprotonated monolayer demonstrates that saccharide size

https://doi.org/10.1021/acsearthspacechem.2c00066
ACS Earth Space Chem. XXXX, XXX, XXX−XXX

impacts the co-adsorption mechanism, organization, and morphology within sea surface microlayer proxy films. Therefore, we have shown that monosaccharides alone are insufficient to accurately model saccharide transport and enrichment in the sea surface microlayer. From this work, we provide Langmuir adsorption fitting parameters of both glucuronate and alginate co-adsorption to a stearic acid monolayer for implementation within marine systems.

■ ASSOCIATED CONTENT

Supporting Information

The Supporting Information is available free of charge at https://pubs.acs.org/doi/10.1021/acsearthspacechem.2c00066.

BAM images of alginate and glucuronate co-adsorption to a stearic acid monolayer as a function of concentration taken during Langmuir surface pressure area isotherms, Langmuir adsorption fitting residual, peak and normalized peak areas of the OH stretching region of stearic-d_{35} acid monolayer on glucuronate containing solutions, CD_2 stretching region spectra of a stearic acid monolayer of the proxy aqueous solution containing (a) alginate and (b) glucuronate at various concentrations, peak area of the CD_2 scissoring mode at 1089 cm^{-1} of stearic-d_{35} acid monolayer on glucuronate containing aqueous solutions, peak area of the ν_S (CD_2) and ν_{AS} (CD_2) modes at 2089 and 2193 cm^{-1} of stearic-d_{35} acid monolayer on glucuronate containing aqueous solutions (PDF)

■ AUTHOR INFORMATION

Corresponding Author

Heather C. Allen − *Department of Chemistry & Biochemistry, The Ohio State University, Columbus, Ohio 43210, United States;* orcid.org/0000-0003-3120-6784; Phone: +1-614-292-4707; Email: allen@chemistry.ohio-state.edu; Fax: +1-614-292-1685

Authors

Maria G. Vazquez de Vasquez − *Department of Chemistry & Biochemistry, The Ohio State University, Columbus, Ohio 43210, United States*

Mickey M. Rogers − *Department of Chemistry & Biochemistry, The Ohio State University, Columbus, Ohio 43210, United States*

Kimberly A. Carter-Fenk − *Department of Chemistry, Stanford University, Stanford, California 94305, United States;* orcid.org/0000-0003-0071-7127

Complete contact information is available at: https://pubs.acs.org/10.1021/acsearthspacechem.2c00066

Author Contributions

M.G.V.d.V. designed the study and H.C.A. supervised the project. M.G.V.d.V performed the experiments. M.G.V.d.V. analyzed the data. M.G.V.d.V. and M.M.R. performed the monolayer thickness calculations. M.G.V.d.V., M.M.R, and K.A.C.-F. wrote and edited the paper with input from all authors.

Notes

The authors declare no competing financial interest.

■ ACKNOWLEDGMENTS

All authors acknowledge funding from the National Science Foundation Center for Aerosol Impacts on Chemistry of the Environment (NSF-CAICE) under Award No. CHE-1801971. M.G.V.d.V. thanks B. Vasquez and R. B. Vasquez for their support throughout the project. M.G.V.d.V. also thanks F. de J. Vazquez de Alba and M. D. Vazquez de Alba for their cover art background image contribution. M.M.R. thanks B. Rogers for thoughtful input and contributions.

■ REFERENCES

(1) Hasenecz, E. S.; Jayarathne, T.; Pendergraft, M. A.; Santander, M. V.; Mayer, K. J.; Sauer, J.; Lee, C.; Gibson, W. S.; Kruse, S. M.; Malfatti, F.; Prather, K. A.; Stone, E. A. Marine Bacteria Affect Saccharide Enrichment in Sea Spray Aerosol during a Phytoplankton Bloom. *ACS Earth Space Chem.* **2020**, *4*, 1638−1649.

(2) Zeppenfeld, S.; van Pinxteren, M.; van Pinxteren, D.; Wex, H.; Berdalet, E.; Vaqué, D.; Dall'Osto, M.; Herrmann, H. Aerosol Marine Primary Carbohydrates and Atmospheric Transformation in the Western Antarctic Peninsula. *ACS Earth Space Chem.* **2021**, *5*, 1032−1047.

(3) Jayarathne, T.; Sultana, C. M.; Lee, C.; Malfatti, F.; Cox, J. L.; Pendergraft, M. A.; Moore, K. A.; Azam, F.; Tivanski, A. V.; Cappa, C. D.; Bertram, T. H.; Grassian, V. H.; Prather, K. A.; Stone, E. A. Enrichment of Saccharides and Divalent Cations in Sea Spray Aerosol During Two Phytoplankton Blooms. *Environ. Sci. Technol.* **2016**, *50*, 11511−11520.

(4) Russell, L. M.; Hawkins, L. N.; Frossard, A. A.; Quinn, P. K.; Bates, T. S. Carbohydrate-like Composition of Submicron Atmospheric Particles and Their Production from Ocean Bubble Bursting. *Proc. Natl. Acad. Sci. U.S.A.* **2010**, *107*, 6652−6657.

(5) Rastelli, E.; Corinaldesi, C.; Dell'Anno, A.; Lo Martire, M.; Greco, S.; Cristina Facchini, M.; Rinaldi, M.; O'Dowd, C.; Ceburnis, D.; Danovaro, R. Transfer of Labile Organic Matter and Microbes from the Ocean Surface to the Marine Aerosol: An Experimental Approach. *Sci. Rep.* **2017**, *7*, No. 11475.

(6) Burrows, S. M.; Gobrogge, E.; Fu, L.; Link, K.; Elliott, S. M.; Wang, H.; Walker, R. OCEANFILMS-2: Representing Coadsorption of Saccharides in Marine Films and Potential Impacts on Modeled Marine Aerosol Chemistry. *Geophys. Res. Lett.* **2016**, *43*, 8306−8313.

(7) Cravigan, L. T.; Mallet, M. D.; Vaattovaara, P.; Harvey, M. J.; Law, C. S.; Modini, R. L.; Russell, L. M.; Stelcer, E.; Cohen, D. D.; Olsen, G.; Safi, K.; Burrell, T. J.; Ristovski, Z. Sea Spray Aerosol Organic Enrichment, Water Uptake and Surface Tension Effects. *Atmos. Chem. Phys.* **2020**, *20*, 7955−7977.

(8) Mopper, K.; zhou, J.; Sri Ramana, K.; passow, U.; dam, H. G.; Drapeau, D. T. The Role of Surface-Active Carbohydrates in the Flocculation of a Diatom Bloom in a Mesocosm. *Deep Sea Res., Part II* **1995**, *42*, 47−73.

(9) Frossard, A. A.; Russell, L. M.; Burrows, S. M.; Elliott, S. M.; Bates, T. S.; Quinn, P. K. Sources and Composition of Submicron Organic Mass in Marine Aerosol Particles. *J. Geophys. Res.: Atmos.* **2014**, *119*, 12977−13003.

(10) Gao, Q.; Leck, C.; Rauschenberg, C.; Matrai, P. A. On the Chemical Dynamics of Extracellular Polysaccharides in the High Arctic Surface Microlayer. *Ocean Sci.* **2012**, *8*, 401−418.

(11) Zhou, J.; Mopper, K.; Passow, U. The Role of Surface-Active Carbohydrates in the Formation of Transparent Exopolymer Particles by Bubble Adsorption of Seawater. *Limnol. Oceanogr.* **1998**, *43*, 1860−1871.

(12) Elliott, S.; Burrows, S. M.; Deal, C.; Liu, X.; Long, M.; Ogunro, O.; Russell, L. M.; Wingenter, O. Prospects for Simulating Macromolecular Surfactant Chemistry at the Ocean−Atmosphere Boundary. *Environ. Res. Lett.* **2014**, *9*, No. 064012.

(13) Burrows, S. M.; Ogunro, O.; Frossard, A. A.; Russell, L. M.; Rasch, P. J.; Elliott, S. M. A Physically Based Framework for Modeling

the Organic Fractionation of Sea Spray Aerosol from Bubble Film Langmuir Equilibria. *Atmos. Chem. Phys.* **2014**, *14*, 13601−13629.
(14) Mochida, M.; Kitamori, Y.; Kawamura, K.; Nojiri, Y.; Suzuki, K. Fatty Acids in the Marine Atmosphere: Factors Governing Their Concentrations and Evaluation of Organic Films on Sea-Salt Particles. *J. Geophys. Res.: Atmos.* **2002**, *107*, AAC 1-1−AAC 1-10.
(15) Hoffman, E. J.; Duce, R. A. Factors Influencing the Organic Carbon Content of Marine Aerosols: A Laboratory Study. *J. Geophys. Res.* **1976**, *81*, 3667−3670.
(16) Collins, D. B.; Bertram, T. H.; Sultana, C. M.; Lee, C.; Axson, J. L.; Prather, K. A. Phytoplankton Blooms Weakly Influence the Cloud Forming Ability of Sea Spray Aerosol. *Geophys. Res. Lett.* **2016**, *43*, 9975−9983.
(17) Forestieri, S. D.; Cornwell, G. C.; Helgestad, T. M.; Moore, K. A.; Lee, C.; Novak, G. A.; Sultana, C. M.; Wang, X.; Bertram, T. H.; Prather, K. A.; Cappa, C. D. Linking Variations in Sea Spray Aerosol Particle Hygroscopicity to Composition during Two Microcosm Experiments. *Atmos. Chem. Phys.* **2016**, *16*, 9003−9018.
(18) Perkins, R. J.; Vazquez de Vasquez, M. G.; Beasley, E. E.; Hill, T. C. J.; Stone, E. A.; Allen, H. C.; DeMott, P. J. Relating Structure and Ice Nucleation of Mixed Surfactant Systems Relevant to Sea Spray Aerosol. *J. Phys. Chem. A* **2020**, *124*, 8806−8821.
(19) Collins, D. B.; Zhao, D. F.; Ruppel, M. J.; Laskina, O.; Grandquist, J. R.; Modini, R. L.; Stokes, M. D.; Russell, L. M.; Bertram, T. H.; Grassian, V. H.; Deane, G. B.; Prather, K. A. Direct Aerosol Chemical Composition Measurements to Evaluate the Physicochemical Differences between Controlled Sea Spray Aerosol Generation Schemes. *Atmos. Meas. Tech.* **2014**, *7*, 3667−3683.
(20) Modini, R. L.; Russell, L. M.; Deane, G. B.; Stokes, M. D. Effect of Soluble Surfactant on Bubble Persistence and Bubble-Produced Aerosol Particles. *J. Geophys. Res.: Atmos.* **2013**, *118*, 1388−1400.
(21) Wonaschütz, A.; Coggon, M.; Sorooshian, A.; Modini, R.; Frossard, A. A.; Ahlm, L.; Mülmenstädt, J.; Roberts, G. C.; Russell, L. M.; Dey, S.; Brechtel, F. J.; Seinfeld, J. H. Hygroscopic Properties of Smoke-Generated Organic Aerosol Particles Emitted in the Marine Atmosphere. *Atmos. Chem. Phys.* **2013**, *13*, 9819−9835.
(22) Leck, C.; Bigg, E. K. Biogenic Particles in the Surface Microlayer and Overlaying Atmosphere in the Central Arctic Ocean during Summer. *Tellus B* **2005**, *57*, 305−316.
(23) Orellana, M. V.; Matrai, P. A.; Leck, C.; Rauschenberg, C. D.; Lee, A. M.; Coz, E. Marine Microgels as a Source of Cloud Condensation Nuclei in the High Arctic. *Proc. Natl. Acad. Sci. U.S.A.* **2011**, *108*, 13612−13617.
(24) Leck, C.; Gao, Q.; Mashayekhy Rad, F.; Nilsson, U. Size-Resolved Atmospheric Particulate Polysaccharides in the High Summer Arctic. *Atmos. Chem. Phys.* **2013**, *13*, 12573−12588.
(25) Leck, C.; Svensson, E. Importance of Aerosol Composition and Mixing State for Cloud Droplet Activation over the Arctic Pack Ice in Summer. *Atmos. Chem. Phys.* **2015**, *15*, 2545−2568.
(26) Zeppenfeld, S.; van Pinxteren, M.; Hartmann, M.; Bracher, A.; Stratmann, F.; Herrmann, H. Glucose as a Potential Chemical Marker for Ice Nucleating Activity in Arctic Seawater and Melt Pond Samples. *Environ. Sci. Technol.* **2019**, *53*, 8747−8756.
(27) Wolf, M. J.; Coe, A.; Dove, L. A.; Zawadowicz, M. A.; Dooley, K.; Biller, S. J.; Zhang, Y.; Chisholm, S. W.; Cziczo, D. J. Investigating the Heterogeneous Ice Nucleation of Sea Spray Aerosols Using Prochlorococcus as a Model Source of Marine Organic Matter. *Environ. Sci. Technol.* **2019**, *53*, 1139−1149.
(28) Hiranuma, N.; Augustin-Bauditz, S.; Bingemer, H.; Budke, C.; Curtius, J.; Danielczok, A.; Diehl, K.; Dreischmeier, K.; Ebert, M.; Frank, F.; Hoffmann, N.; Kandler, K.; Kiselev, A.; Koop, T.; Leisner, T.; Möhler, O.; Nillius, B.; Peckhaus, A.; Rose, D.; Weinbruch, S.; Wex, H.; Boose, Y.; DeMott, P. J.; Hader, J. D.; Hill, T. C. J.; Kanji, Z. A.; Kulkarni, G.; Levin, E. J. T.; McCluskey, C. S.; Murakami, M.; Murray, B. J.; Niedermeier, D.; Petters, M. D.; O' Sullivan, D.; Saito, A.; Schill, G. P.; Tajiri, T.; Tolbert, M. A.; Welti, A.; Whale, T. F.; Wright, T. P.; Yamashita, K. A Comprehensive Laboratory Study on the Immersion Freezing Behavior of Illite NX Particles: A Comparison of 17 Ice Nucleation Measurement Techniques. *Atmos. Chem. Phys.* **2015**, *15*, 2489−2518.
(29) Dreischmeier, K.; Budke, C.; Wiehemeier, L.; Kottke, T.; Koop, T. Boreal Pollen Contain Ice-Nucleating as Well as Ice-Binding 'Antifreeze' Polysaccharides. *Sci. Rep.* **2017**, *7*, No. 41890.
(30) Wilson, T. W.; Ladino, L. A.; Alpert, P. A.; Breckels, M. N.; Brooks, I. M.; Browse, J.; Burrows, S. M.; Carslaw, K. S.; Huffman, J. A.; Judd, C.; Kilthau, W. P.; Mason, R. H.; McFiggans, G.; Miller, L. A.; Najera, J. J.; Polishchuk, E.; Rae, S.; Schiller, C. L.; Si, M.; Temprado, J. V.; Whale, T. F.; Wong, J. P. S.; Wurl, O.; Yakobi-Hancock, J. D.; Abbatt, J. P. D.; Aller, J. Y.; Bertram, A. K.; Knopf, D. A.; Murray, B. J. A Marine Biogenic Source of Atmospheric Ice-Nucleating Particles. *Nature* **2015**, *525*, 234−238.
(31) Pummer, B. G.; Budke, C.; Augustin-Bauditz, S.; et al. Ice Nucleation by Water-Soluble Macromolecules. *Atmos. Chem. Phys.* **2015**, *15*, 4077−4091.
(32) Hiranuma, N.; Möhler, O.; Yamashita, K.; Tajiri, T.; Saito, A.; Kiselev, A.; Hoffmann, N.; Hoose, C.; Jantsch, E.; Koop, T.; Murakami, M. Ice Nucleation by Cellulose and Its Potential Contribution to Ice Formation in Clouds. *Nat. Geosci.* **2015**, *8*, 273−277.
(33) Pummer, B. G.; Bauer, H.; Bernardi, J.; Bleicher, S.; Grothe, H. Suspendable Macromolecules Are Responsible for Ice Nucleation Activity of Birch and Conifer Pollen. *Atmos. Chem. Phys.* **2012**, *12*, 2541−2550.
(34) Cochran, R. E.; Jayarathne, T.; Stone, E. A.; Grassian, V. H. Selectivity Across the Interface: A Test of Surface Activity in the Composition of Organic-Enriched Aerosols from Bubble Bursting. *J. Phys. Chem. Lett.* **2016**, *7*, 1692−1696.
(35) O'Dowd, C. D.; de Leeuw, G. Marine Aerosol Production: A Review of the Current Knowledge. *Philos. Trans. R. Soc., A* **2007**, *365*, 1753−1774.
(36) Quinn, P. K.; Bates, T. S.; Schulz, K. S.; Coffman, D. J.; Frossard, A. A.; Russell, L. M.; Keene, W. C.; Kieber, D. J. Contribution of Sea Surface Carbon Pool to Organic Matter Enrichment in Sea Spray Aerosol. *Nat. Geosci.* **2014**, *7*, 228−232.
(37) Sanchez, K. J.; Russell, L. M.; Modini, R. L.; Frossard, A. A.; Ahlm, L.; Corrigan, C. E.; Roberts, G. C.; Hawkins, L. N.; Schroder, J. C.; Bertram, A. K.; Zhao, R.; Lee, A. K. Y.; Lin, J. J.; Nenes, A.; Wang, Z.; Wonaschütz, A.; Sorooshian, A.; Noone, K. J.; Jonsson, H.; Toom, D.; Macdonald, A. M.; Leaitch, W. R.; Seinfeld, J. H. Meteorological and Aerosol Effects on Marine Cloud Microphysical Properties. *J. Geophys. Res.: Atmos.* **2016**, *121*, 4142−4161.
(38) Modini, R. L.; Frossard, A. A.; Ahlm, L.; Russell, L. M.; Corrigan, C. E.; Roberts, G. C.; Hawkins, L. N.; Schroder, J. C.; Bertram, A. K.; Zhao, R.; Lee, A. K. Y.; Abbatt, J. P. D.; Lin, J.; Nenes, A.; Wang, Z.; Wonaschütz, A.; Sorooshian, A.; Noone, K. J.; Jonsson, H.; Seinfeld, J. H.; Toom-Sauntry, D.; Macdonald, A. M.; Leaitch, W. R. Primary Marine Aerosol-cloud Interactions off the Coast of California. *J. Geophys. Res.: Atmos.* **2015**, *120*, 4282−4303.
(39) Verdugo, P.; Alldredge, A. L.; Azam, F.; Kirchman, D. L.; Passow, U.; Santschi, P. H. The Oceanic Gel Phase: A Bridge in the DOM−POM Continuum. *Mar. Chem.* **2004**, *92*, 67−85.
(40) Azam, F.; Malfatti, F. Microbial Structuring of Marine Ecosystems. *Nat. Rev. Microbiol.* **2007**, *5*, 782−791.
(41) Verdugo, P.; Orellana, M. V.; Chin, W.-C.; Petersen, T. W.; van den Eng, G.; Benner, R.; Hedges, J. I. Marine Biopolymer Self-Assembly: Implications for Carbon Cycling in the Ocean. *Faraday Discuss.* **2008**, *139*, 393−398.
(42) Verdugo, P. Marine Microgels. *Annu. Rev. Mar. Sci.* **2012**, *4*, 375−400.
(43) Galgani, L.; Piontek, J.; Engel, A. Biopolymers Form a Gelatinous Microlayer at the Air-Sea Interface When Arctic Sea Ice Melts. *Sci. Rep.* **2016**, *6*, No. 29465.
(44) Tanaka, T.; Fillmore, D.; Sun, S.-T.; Nishio, I.; Swislow, G.; Shah, A. Phase Transitions in Ionic Gels. *Phys. Rev. Lett.* **1980**, *45*, 1636−1639.
(45) Verdugo, P. Dynamics of Marine Biopolymer Networks. *Polym. Bull.* **2007**, *58*, 139−143.

https://doi.org/10.1021/acsearthspacechem.2c00066
ACS Earth Space Chem. XXXX, XXX, XXX−XXX

(46) Link, K. A.; Spurzem, G. N.; Tuladhar, A.; Chase, Z.; Wang, Z.; Wang, H.; Walker, R. A. Organic Enrichment at Aqueous Interfaces: Cooperative Adsorption of Glucuronic Acid to DPPC Monolayers Studied with Vibrational Sum Frequency Generation. *J. Phys. Chem. A* **2019**, *123*, 5621−5632.
(47) Hasenecz, E. S.; Kaluarachchi, C. P.; Lee, H. D.; Tivanski, A. V.; Stone, E. A. Saccharide Transfer to Sea Spray Aerosol Enhanced by Surface Activity, Calcium, and Protein Interactions. *ACS Earth Space Chem.* **2019**, *3*, 2539−2548.
(48) de Moura, M. R.; Ahmad Aouada, F.; Favaro, S. L.; Radovanovic, E.; Forti Rubira, A.; Muniz, E. C. Release of BSA from Porous Matrices Constituted of Alginate−Ca2+ and PNIPAAm-Interpenetrated Networks. *Mater. Sci. Eng., C* **2009**, *29*, 2319−2325.
(49) Lin, J. D.; Lemay, M. A.; Parfrey, L. W. Diverse Bacteria Utilize Alginate Within the Microbiome of the Giant Kelp Macrocystis Pyrifera. *Front. Microbiol.* **2018**, *9*, No. 1914.
(50) Zhang, L.; Li, X.; Zhang, X.; Li, Y.; Wang, L. Bacterial Alginate Metabolism: An Important Pathway for Bioconversion of Brown Algae. *Biotechnol. Biofuels* **2021**, *14*, No. 158.
(51) Jain, S.; Ohman, D. E. Role of an Alginate Lyase for Alginate Transport in Mucoid *Pseudomonas aeruginosa*. *Infect. Immun.* **2005**, *73*, 6429−6436.
(52) Thomas, F.; Barbeyron, T.; Tonon, T.; Génicot, S.; Czjzek, M.; Michel, G. Characterization of the First Alginolytic Operons in a Marine Bacterium: From Their Emergence in Marine Flavobacteriia to Their Independent Transfers to Marine Proteobacteria and Human Gut Bacteroides. *Environ. Microbiol.* **2012**, *14*, 2379−2394.
(53) Hassler, C. S.; Schoemann, V.; Nichols, C. M.; Butler, E. C. V.; Boyd, P. W. Saccharides Enhance Iron Bioavailability to Southern Ocean Phytoplankton. *Proc. Natl. Acad. Sci. U.S.A.* **2011**, *108*, 1076−1081.
(54) Carter-Fenk, K. A.; Dommer, A. C.; Fiamingo, M. E.; Kim, J.; Amaro, R. E.; Allen, H. C. Calcium Bridging Drives Polysaccharide Co-Adsorption to a Proxy Sea Surface Microlayer. *Phys. Chem. Chem. Phys.* **2021**, *23*, 16401−16416.
(55) Cochran, R. E.; Laskina, O.; Jayarathne, T.; Laskin, A.; Laskin, J.; Lin, P.; Sultana, C.; Lee, C.; Moore, K. A.; Cappa, C. D.; Bertram, T. H.; Prather, K. A.; Grassian, V. H.; Stone, E. A. Analysis of Organic Anionic Surfactants in Fine and Coarse Fractions of Freshly Emitted Sea Spray Aerosol. *Environ. Sci. Technol.* **2016**, *50*, 2477−2486.
(56) Ralston, A. W.; Hoerr, C. W. The solubilities of the normal saturated fatty acids. *J. Org. Chem.* **1942**, *07*, 546−555.
(57) Hua, W.; Verreault, D.; Adams, E. M.; Huang, Z.; Allen, H. C. Impact of Salt Purity on Interfacial Water Organization Revealed by Conventional and Heterodyne-Detected Vibrational Sum Frequency Generation Spectroscopy. *J. Phys. Chem. C* **2013**, *117*, 19577−19585.
(58) Huang, Z.; Hua, W.; Verreault, D.; Allen, H. C. Influence of Salt Purity on Na+ and Palmitic Acid Interactions. *J. Phys. Chem. A* **2013**, *117*, 13412−13418.
(59) Adel, T.; Ng, K. C.; Vazquez de Vasquez, M. G.; Velez-Alvarez, J.; Allen, H. C. Insight into the Ionizing Surface Potential Method and Aqueous Sodium Halide Surfaces. *Langmuir* **2021**, *37*, 7863−7874.
(60) Adams, E. M.; Allen, H. C. Palmitic Acid on Salt Subphases and in Mixed Monolayers of Cerebrosides: Application to Atmospheric Aerosol Chemistry. *Atmosphere* **2013**, *4*, 315−336.
(61) Griffith, E. C.; Adams, E. M.; Allen, H. C.; Vaida, V. Hydrophobic Collapse of a Stearic Acid Film by Adsorbed L-Phenylalanine at the Air−Water Interface. *J. Phys. Chem. B* **2012**, *116*, 7849−7857.
(62) Neal, J. F.; Zhao, W.; Grooms, A. J.; Flood, A. H.; Allen, H. C. Arginine−Phosphate Recognition Enhanced in Phospholipid Monolayers at Aqueous Interfaces. *J. Phys. Chem. C* **2018**, *122*, 26362−26371.
(63) Adams, E. M.; Casper, C. B.; Allen, H. C. Effect of Cation Enrichment on Dipalmitoylphosphatidylcholine (DPPC) Monolayers at the Air-Water Interface. *J. Colloid Interface Sci.* **2016**, *478*, 353−364.
(64) Adams, E. M.; Verreault, D.; Jayarathne, T.; Cochran, R. E.; Stone, E. A.; Allen, H. C. Surface Organization of a DPPC Monolayer on Concentrated SrCl2 and ZnCl2 Solutions. *Phys. Chem. Chem. Phys.* **2016**, *18*, 32345−32357.
(65) Vazquez de Vasquez, M. G.; Carter-Fenk, K. A.; McCaslin, L. M.; Beasley, E. E.; Clark, J. B.; Allen, H. C. Hydration and Hydrogen Bond Order of Octadecanoic Acid and Octadecanol Films on Water at 21 and 1 °C. *J. Phys. Chem. A* **2021**, *125*, 10065−10078.
(66) Auvil, N. C.; Vazquez de Vasquez, M. G.; Allen, H. C. Zinc−Carboxylate Binding in Mixed Octadecanoic Acid and Octadecanol Monolayers on Proxy Seawater Solution Surfaces. *ACS Earth Space Chem.* **2021**, *5*, 2947−2956.
(67) Vazquez de Vasquez, M. G.; Wellen Rudd, B. A.; Baer, M. D.; Beasley, E. E.; Allen, H. C. Role of Hydration in Magnesium versus Calcium Ion Pairing with Carboxylate: Solution and the Aqueous Interface. *J. Phys. Chem. B* **2021**, *125*, 11308−11319.
(68) Buffeteau, T.; Desbat, B.; Eyquem, D. Attenuated Total Reflection Fourier Transform Infrared Microspectroscopy: Theory and Application to Polymer Samples. *Vib. Spectrosc.* **1996**, *11*, 29−36.
(69) Flach, C. R.; Gericke, A.; Mendelsohn, R. Quantitative Determination of Molecular Chain Tilt Angles in Monolayer Films at the Air/Water Interface: Infrared Reflection/Absorption Spectroscopy of Behenic Acid Methyl Ester. *J. Phys. Chem. B* **1997**, *101*, 58−65.
(70) Gericke, A.; Huehnerfuss, H. In Situ Investigation of Saturated Long-Chain Fatty Acids at the Air/Water Interface by External Infrared Reflection-Absorption Spectrometry. *J. Phys. Chem. A* **1993**, *97*, 12899−12908.
(71) Mendelsohn, R.; Flach, C. R. Infrared Reflection−Absorption Spectrometry of Monolayer Films at the Air−Water Interface. In *Handbook of Vibrational Spectroscopy*; American Cancer Society, 2006. https://doi.org/10.1002/0470027320.s2205.
(72) Shanmukh, S.; Biswas, N.; Waring, A. J.; Walther, F. J.; Wang, Z.; Chang, Y.; Notter, R. H.; Dluhy, R. A. Structure and Properties of Phospholipid−Peptide Monolayers Containing Monomeric SP-B1−25: II. Peptide Conformation by Infrared Spectroscopy. *Biophys. Chem.* **2005**, *113*, 233−244.
(73) Mandalakis, M.; Stephanou, E. G. Study of Atmospheric PCB Concentrations over the Eastern Mediterranean Sea. *J. Geophys. Res.: Atmos.* **2002**, *107*, ACH 18-1−ACH 18-14.
(74) Mashayekhy Rad, F.; Leck, C.; Ilag, L. L.; Nilsson, U. Investigation of Ultrahigh-Performance Liquid Chromatography/Travelling-Wave Ion Mobility/Time-of-Flight Mass Spectrometry for Fast Profiling of Fatty Acids in the High Arctic Sea Surface Microlayer. *Rapid Commun. Mass Spectrom.* **2018**, *32*, 942−950.
(75) Quinn, P. K.; Collins, D. B.; Grassian, V. H.; Prather, K. A.; Bates, T. S. Chemistry and Related Properties of Freshly Emitted Sea Spray Aerosol. *Chem. Rev.* **2015**, *115*, 4383−4399.
(76) Dean Pakulski, J.; Benner, R. An Improved Method for the Hydrolysis and MBTH Analysis of Dissolved and Particulate Carbohydrates in Seawater. *Mar. Chem.* **1992**, *40*, 143−160.
(77) Patil, G. S.; Matthews, R. H.; Cornwell, D. G. Effect of Ionization and Cation Selectivity on the Expansion of Stearic Acid Monolayers. *J. Lipid Res.* **1972**, *13*, 574−579.
(78) Sears, D. F.; Schulman, J. H. Influence of Water Structures on the Surface Pressure, Surface Potential, and Area of Soap Monolayers of Lithium, Sodium, Potassium, and Calcium. *J. Phys. Chem. C* **1964**, *68*, 3529−3534.
(79) Neal, J. F.; Rogers, M. M.; Smeltzer, M. A.; Carter-Fenk, K. A.; Grooms, A. J.; Zerkle, M. M.; Allen, H. C. Sodium Drives Interfacial Equilibria for Semi-Soluble Phosphoric and Phosphonic Acids of Model Sea Spray Aerosol Surfaces. *ACS Earth Space Chem.* **2020**, *4*, 1549−1557.
(80) Carter-Fenk, K. A.; Allen, H. C. Collapse Mechanisms of Nascent and Aged Sea Spray Aerosol Proxy Films. *Atmosphere* **2018**, *9*, No. 503.
(81) Gaines, G. L. *Insoluble Monolayers at Liquid-Gas Interfaces*; Interscience Publishers: New York, NY, USA, 1966.
(82) Butt, H.-J.; Graf, K.; Kappl, M. *Physics and Chemistry of Interfaces*; John Wiley & Sons, 2013.

(83) Adams, E. M.; Wellen, B. A.; Thiraux, R.; Reddy, S. K.; Vidalis, A. S.; Paesani, F.; Allen, H. C. Sodium−Carboxylate Contact Ion Pair Formation Induces Stabilization of Palmitic Acid Monolayers at High PH. *Phys. Chem. Chem. Phys.* **2017**, *19*, 10481−10490.
(84) Angelova, A.; Vollhardt, D.; Ionov, R. 2D−3D Transformations of Amphiphilic Monolayers Influenced by Intermolecular Interactions: A Brewster Angle Microscopy Study. *J. Phys. Chem. B* **1996**, *100*, 10710−10720.
(85) Schill, S. R.; Burrows, S. M.; Hasenecz, E. S.; Stone, E. A.; Bertram, T. H. The Impact of Divalent Cations on the Enrichment of Soluble Saccharides in Primary Sea Spray Aerosol. *Atmosphere* **2018**, *9*, No. 476.
(86) Millero, F. J.; Feistel, R.; Wright, D. G.; McDougall, T. J. The Composition of Standard Seawater and the Definition of the Reference-Composition Salinity Scale. *Deep-Sea Res., Part A* **2008**, *55*, 50−72.
(87) Millero, F. J. *Chemical Oceanography*, 4th ed.; CRC Press: Boca Raton, 2013. https://doi.org/10.1201/b14753.
(88) Denton, J. K.; Kelleher, P. J.; Johnson, M. A.; Baer, M. D.; Kathmann, S. M.; Mundy, C. J.; Wellen Rudd, B. A.; Allen, H. C.; Choi, T. H.; Jordan, K. D. Molecular-Level Origin of the Carboxylate Head Group Response to Divalent Metal Ion Complexation at the Air−Water Interface. *Proc. Natl. Acad. Sci. U.S.A.* **2019**, *116*, 14874−14880.
(89) Miranda, P. B.; Du, Q.; Shen, Y. R. Interaction of Water with a Fatty Acid Langmuir Film. *Chem. Phys. Lett.* **1998**, *286*, 1−8.
(90) Kanicky, J. R.; Shah, D. O. Effect of Degree, Type, and Position of Unsaturation on the PKa of Long-Chain Fatty Acids. *J. Colloid Interface Sci.* **2002**, *256*, 201−207.
(91) Heikkila, R. E.; Deamer, D. W.; Cornwell, D. G. Solution of Fatty Acids from Monolayers Spread at the Air-Water Interface: Identification of Phase Transformations and the Estimation of Surface Charge. *J. Lipid Res.* **1970**, *11*, 195−200.
(92) Peters, R. A.; Hinshelwood, C. N. Interfacial Tension and Hydrogen-Ion Concentration. *Proc. R. Soc. London, Ser. A* **1931**, *133*, 140−154.
(93) Kanicky, J. R.; Poniatowski, A. F.; Mehta, N. R.; Shah, D. O. Cooperativity among Molecules at Interfaces in Relation to Various Technological Processes: Effect of Chain Length on the pK_a of Fatty Acid Salt Solutions. *Langmuir* **2000**, *16*, 172−177.
(94) Bu, H.; Kjøniksen, A.-L.; Elgsaeter, A.; Nyström, B. Interaction of Unmodified and Hydrophobically Modified Alginate with Sodium Dodecyl Sulfate in Dilute Aqueous Solution: Calorimetric, Rheological, and Turbidity Studies. *Colloids Surf., A* **2006**, *278*, 166−174.
(95) Wellen Rudd, B. A.; Vidalis, A. S.; Allen, H. C. Thermodynamic versus Non-Equilibrium Stability of Palmitic Acid Monolayers in Calcium-Enriched Sea Spray Aerosol Proxy Systems. *Phys. Chem. Chem. Phys.* **2018**, *20*, 16320−16332.
(96) Luo, M.; Wauer, N. A.; Angle, K. J.; Dommer, A. C.; Song, M.; Nowak, C. M.; Amaro, R. E.; Grassian, V. H. Insights into the Behavior of Nonanoic Acid and Its Conjugate Base at the Air/Water Interface through a Combined Experimental and Theoretical Approach. *Chem. Sci.* **2020**, *11*, 10647−10656.
(97) Tang, C. Y.; Huang, Z.; Allen, H. C. Interfacial Water Structure and Effects of Mg2+ and Ca2+ Binding to the COOH Headgroup of a Palmitic Acid Monolayer Studied by Sum Frequency Spectroscopy. *J. Phys. Chem. B* **2011**, *115*, 34−40.
(98) Tang, C. Y.; Huang, Z.; Allen, H. C. Binding of Mg2+ and Ca2+ to Palmitic Acid and Deprotonation of the COOH Headgroup Studied by Vibrational Sum Frequency Generation Spectroscopy. *J. Phys. Chem. B* **2010**, *114*, 17068−17076.
(99) Tang, C. Y.; Allen, H. C. Ionic Binding of Na+ versus K+ to the Carboxylic Acid Headgroup of Palmitic Acid Monolayers Studied by Vibrational Sum Frequency Generation Spectroscopy. *J. Phys. Chem. A* **2009**, *113*, 7383−7393.
(100) Tang, F.; Ohto, T.; Sun, S.; Rouxel, J. R.; Imoto, S.; Backus, E. H. G.; Mukamel, S.; Bonn, M.; Nagata, Y. Molecular Structure and Modeling of Water−Air and Ice−Air Interfaces Monitored by Sum-Frequency Generation. *Chem. Rev.* **2020**, *120*, 3633−3667.
(101) Balzerowski, P.; Meister, K.; Versluis, J.; Bakker, H. J. Heterodyne-Detected Sum Frequency Generation Spectroscopy of Polyacrylic Acid at the Air/Water-Interface. *Phys. Chem. Chem. Phys.* **2016**, *18*, 2481−2487.
(102) Langmuir, I. The adsorption of gases on plane surfaces of glass, mica and platinum. *J. Am. Chem. Soc.* **1918**, *40*, 1361−1403.
(103) Henry, D. C. L. X. A Kinetic Theory of Adsorption. *London, Edinburgh Dublin Philos. Mag. J. Sci.* **1922**, *44*, 689−705.
(104) Chen, H.; Gan, W.; Lu, R.; Guo, Y.; Wang, H. Determination of Structure and Energetics for Gibbs Surface Adsorption Layers of Binary Liquid Mixture 2. Methanol + Water. *J. Phys. Chem. B* **2005**, *109*, 8064−8075.
(105) Mohammed, C.; Lalgee, L.; Kistow, M.; Jalsa, N.; Ward, K. On the Binding Affinity and Thermodynamics of Sodium Alginate-Heavy Metal Ion Interactions for Efficient Adsorption. *Carbohydr. Polym. Technol. Appl.* **2022**, *3*, No. 100203.
(106) Ayoub, G. T.; Bashara, N. M. Characterization of a Very Thin Uniaxial Film on a Nonabsorbing Substrate by Multiple Wavelength Ellipsometry: Palmitic Acid on Water*. *J. Opt. Soc. Am.* **1978**, *68*, 978−983.
(107) Craig, B. M. Refractive Indices of Some Saturated and Monoethenoid Fatty Acids and Methyl Esters. *Can. J. Chem.* **1953**, *31*, 499−504.
(108) Pusterla, J. M.; Malfatti-Gasperini, A. A.; Puentes-Martinez, X. E.; Cavalcanti, L. P.; Oliveira, R. G. Refractive Index and Thickness Determination in Langmuir Monolayers of Myelin Lipids. *Biochim. Biophys. Acta, Biomembr.* **2017**, *1859*, 924−930.
(109) Winsel, K.; Hönig, D.; Lunkenheimer, K.; Geggel, K.; Witt, C. Quantitative Brewster Angle Microscopy of the Surface Film of Human Broncho-Alveolar Lavage Fluid. *Eur. Biophys. J.* **2003**, *32*, 544−552.
(110) Haynes, W. M. *CRC Handbook of Chemistry and Physics*; CRC Press, 2014.
(111) Rogers, M. M.; Neal, J. F.; Saha, A.; Algarni, A. S.; Hill, T. C. J.; Allen, H. C. The Ocean's Elevator: Evolution of the Air−Seawater Interface during a Small-Scale Algal Bloom. *ACS Earth Space Chem.* **2020**, *4*, 2347−2357.
(112) Kienle, D. F.; de Souza, J. V.; Watkins, E. B.; Kuhl, T. L. Thickness and Refractive Index of DPPC and DPPE Monolayers by Multiple-Beam Interferometry. *Anal. Bioanal. Chem.* **2014**, *406*, 4725−4733.
(113) Reynolds, P. A.; McGillivray, D. J.; Gilbert, E. P.; Holt, S. A.; Henderson, M. J.; White, J. W. Neutron and X-Ray Reflectivity from Polyisobutylene-Based Amphiphiles at the Air−Water Interface. *Langmuir* **2003**, *19*, 752−761.
(114) DeLucas, L.; Bugg, C. E.; Terzis, A.; Rivest, R. Calcium Binding to D-Glucuronate Residues: Crystal Structure of a Hydrated Calcium Bromide Salt of D-Glucuronic Acid. *Carbohydr. Res.* **1975**, *41*, 19−29.
(115) Ferrari, E.; Grandi, R.; Lazzari, S.; Saladini, M. Hg(II)-Coordination by Sugar-Acids: Role of the Hydroxy Groups. *J. Inorg. Biochem.* **2005**, *99*, 2381−2386.
(116) Whitfield, D. M.; Stojkovski, S.; Sarkar, B. Metal Coordination to Carbohydrates. Structures and Function. *Coord. Chem. Rev.* **1993**, *122*, 171−225.
(117) Kundu, S.; Langevin, D. Fatty Acid Monolayer Dissociation and Collapse: Effect of PH and Cations. *Colloids Surf., A* **2008**, *325*, 81−85.
(118) Le Calvez, E.; Blaudez, D.; Buffeteau, T.; Desbat, B. Effect of Cations on the Dissociation of Arachidic Acid Monolayers on Water Studied by Polarization-Modulated Infrared Reflection−Absorption Spectroscopy. *Langmuir* **2001**, *17*, 670−674.
(119) Simon-Kutscher, J.; Gericke, A.; Hühnerfuss, H. Effect of Bivalent Ba, Cu, Ni, and Zn Cations on the Structure of Octadecanoic Acid Monolayers at the Air−Water Interface As Determined by External Infrared Reflection−Absorption Spectroscopy. *Langmuir* **1996**, *12*, 1027−1034.
(120) Wang, Y.; Du, X.; Guo, L.; Liu, H. Chain Orientation and Headgroup Structure in Langmuir Monolayers of Stearic Acid and

Metal Stearate (Ag, Co, Zn, and Pb) Studied by Infrared Reflection-Absorption Spectroscopy. *J. Chem. Phys.* **2006**, *124*, No. 134706.
(121) Link, K. A.; Hsieh, C.-Y.; Tuladhar, A.; Chase, Z.; Wang, Z.; Wang, H.; Walker, R. A. Vibrational Studies of Saccharide-Induced Lipid Film Reorganization at Aqueous/Air Interfaces. *Chem. Phys.* **2018**, *512*, 104−110.
(122) Neal, J. F.; Zhao, W.; Grooms, A. J.; Smeltzer, M. A.; Shook, B. M.; Flood, A. H.; Allen, H. C. Interfacial Supramolecular Structures of Amphiphilic Receptors Drive Aqueous Phosphate Recognition. *J. Am. Chem. Soc.* **2019**, *141*, 7876−7886.
(123) Cameron, D. G.; Casal, H. L.; Gudgin, E. F.; Mantsch, H. H. The Gel Phase of Dipalmitoyl Phosphatidylcholine. An Infrared Characterization of the Acyl Chain Packing. *Biochim. Biophys. Acta, Biomembr.* **1980**, *596*, 463−467.
(124) Mendelsohn, R.; Brauner, J. W.; Gericke, A. External Infrared Reflection Absorption Spectrometry of Monolayer Films at the Air-Water Interface. *Annu. Rev. Phys. Chem.* **1995**, *46*, 305−334.

https://doi.org/10.1021/acsearthspacechem.2c00066
ACS Earth Space Chem. XXXX, XXX, XXX−XXX